



HHS Public Access

Author manuscript

Biochem Pharmacol. Author manuscript; available in PMC 2021 October 01.

Published in final edited form as:

Biochem Pharmacol. 2021 October ; 192: 114688. doi:10.1016/j.bcp.2021.114688.

TTI-101: A competitive inhibitor of STAT3 that spares oxidative phosphorylation and reverses mechanical allodynia in mouse models of neuropathic pain

Moses M. Kasembeli^a, Pooja Singhmar^b, Jiacheng Ma^b, Jules Edralin^b, Yongfu Tang^b, Clydell Adams III^a, Cobi J. Heijnen^b, Annemieke Kavelaars^b, David J. Tweardy^{a,*}

^aThe Department of Infectious Diseases, Infection Control & Employee Health, Division of Internal Medicine, University of Texas MD Anderson Cancer Center, 1515 Holcombe Boulevard, Houston, TX 77030-4009, United States

^bThe Department of Symptom Research, Division of Internal Medicine, University of Texas MD Anderson Cancer Center, 1515 Holcombe Boulevard, Houston, TX 77030-4009, United States

Abstract

Signal Transducer and Activator of Transcription (STAT) 3 emerged rapidly as a high-value target for treatment of cancer. However, small-molecule STAT3 inhibitors have been slow to enter the clinic due, in part, to serious adverse events (SAE), including lactic acidosis and peripheral neuropathy, which have been attributed to inhibition of STAT3's mitochondrial function. Our group developed TTI-101, a competitive inhibitor of STAT3 that targets the receptor pY705-peptide binding site within the Src homology 2 (SH2) domain to block its recruitment and activation. TTI-101 has shown target engagement, no toxicity, and evidence of clinical benefit in a Phase I study in patients with solid tumors. Here we report that TTI-101 did not affect mitochondrial function, nor did it cause STAT3 aggregation, chemically modify STAT3 or cause neuropathic pain. Instead, TTI-101 unexpectedly suppressed neuropathic pain induced by chemotherapy or in a spared nerve injury model. Thus, in addition to its direct anti-tumor effect, TTI-101 may be of benefit when administered to cancer patients at risk of developing chemotherapy-induced peripheral neuropathy (CIPN).

Keywords

STAT3; neuropathic pain; allodynia; CIPN; TTI-101; VEGF

This is an open access article under the CC BY-NC-ND license (<http://creativecommons.org/licenses/by-nc-nd/4.0/>).

*Corresponding author. djtweardy@mdanderson.org (D.J. Tweardy).

Declaration of Competing Interest

Baylor College of Medicine, with David Tweardy as inventor, has filed 8 patent families covering the use of TTI-101, a small-molecule inhibitor of STAT3 used in this study. These patents are exclusively licensed to Tvardi Therapeutics, Inc., in which David Tweardy owns stock.

1. Introduction

STAT3 is known to play an essential role in biological processes important for development, including cell growth and survival, as well as in restoring homeostasis after injury. However, persistent STAT3 signaling has been linked to a number of pathological conditions including cancer, chronic inflammation and fibrosis. An extensive body of preclinical data indicates that inhibition of STAT3 signaling may be of substantial therapeutic benefit [1,2]. However, agents that target STAT3 have been slow to enter the clinic, in part, because of difficulties inherent in targeting transcription factors, a class of proteins deemed “undruggable” due to the large size of their protein–protein interaction interfaces [3]. In addition, serious adverse events (SAE), including lactic acidosis and peripheral neuropathy, have been observed with some small-molecule STAT3 inhibitors in clinical-stage development [4,5]. These have been attributed to targeting of STAT3’s non-canonical functions, most notably, its contribution to mitochondrial-mediated oxidative phosphorylation [6], which relies on phosphorylation of STAT3 on serine 727, in contrast to phosphorylation on tyrosine 705 required for its canonical function [7,8].

Many STAT3-directed drug development programs have focused on STAT3’s SH2 domain, in particular its phosphotyrosine (pY) peptide binding pocket. However, the finding that some inhibitors induce mitochondrial toxicity suggests they may target other regions of STAT3 and affect STAT3 structure and stability. In fact, Genini et al. demonstrated that OPB-51602, and other small-molecule STAT3 inhibitors designed to directly target STAT3, caused STAT3 aggregation and altered intracellular protein homeostasis [6]. They further argued that induction of cell death by these agents is mediated, in part, through a proteotoxic mechanism in metabolically stressed cancer cells and suggested that this may be a common mechanism underlying the anticancer activity of any inhibitor that directly targets the SH2 domain within STAT3.

Our group, working in collaboration with Tvardi Therapeutics, Inc., developed TTI-101 (formerly C188–9), a competitive inhibitor of STAT3 designed to target the pY-peptide binding site within STAT3’s SH2 domain and thereby directly block two key steps in its activation—recruitment to activated cytokine receptor complexes and homodimerization [9,10]. We previously performed good laboratory practice (GLP)-compliant, 28-day pharmacotoxicology studies of TTI-101 [10] that demonstrated no drug-related toxicity up to the maximum dose administered (200 mg/kg/day in rats and 100 mg/kg/day in dogs). Moreover, an ongoing Phase I clinical trial of TTI-101 that has enrolled 40 patients with advanced solid tumors [11] up to dose level 4 (25.6 mg/kg/day) for as long as 12 months, has not demonstrated any serious adverse events, including lactic acidosis.

The studies reported here were undertaken to determine *in vitro* if TTI-101 affects STAT3 mitochondrial function, causes STAT3 aggregation, chemically modifies STAT3, or induces peripheral neuropathy in mice. We tested TTI-101 and four other STAT3 inhibitors purported to target the STAT3 SH2 domain and demonstrated that two of these—WP-1066 and cryptotanshinone—induced STAT3 aggregation and caused mitochondrial toxicity in metabolically stressed cells. Importantly, our studies revealed that TTI-101 does not: 1) affect mitochondrial function, 2) chemically modify STAT3, 3) cause STAT3 aggregation

in metabolically stressed cells, or 4) cause peripheral neuropathy. In fact, TTI-101 administration unexpectedly reversed mechanical allodynia in models of chemotherapy-induced peripheral neuropathy (CIPN) and spared nerve injury (SNI). These findings indicate that TTI-101 may be of special benefit when administered to patients receiving CIPN-inducing agents as part of their cancer therapy regimen.

2. Material and methods

2.1. Materials

STAT3 inhibitors - Stattic, cryptotanshinone, WP1066 and STA21 were obtained from Selleck Chemicals (Houston, TX, USA). TTI-101 was custom synthesized by Regis technologies Inc. (Morton Grove, IL, USA). Molecular grade dimethyl sulfoxide (DMSO), reduced glutathione (GSH), iodoacetamide, and N-ethylmaleimide were obtained from Sigma-Aldrich (St. Louis, MO, USA). Cisplatin was acquired from (TEVA Pharmaceuticals, North Wales, PA). All LC/MS reagents, including ammonium acetate, formic acid, acetonitrile, methanol and water, were obtained from Honeywell Fluka (Morris Plains, NJ, USA). STAT3 antibody was purchased from Cell Signaling Technology (Danvers, MA, USA). Antibodies to histone H2B (ab52484) and GAPDH (ab9485) were purchased from Abcam (Toronto, ON, Canada). Antibody to Vimentin (sc66002) was obtained from Santa Cruz Biotechnology (Dallas, TX, USA). DMEM XF base medium, FCCP, and rotenone/antimycin A were obtained from Agilent Technologies (Santa Clara, CA, USA). A C18 Synergi™ 4 µm Fusion-RP 80 Å LC column (50 × 2 mm) was purchased from Phenomenex, (Torrance, CA, USA); a Waters Symmetry C18 column (100 Å, 3.5 µm, 4.6 mm × 150 mm) was purchased from Waters (Milford, MA, USA).

2.2. Cell line and culture

The human prostate cancer cell line DU-145 was obtained from American Type Culture Collection (ATCC, Rockville, MD, USA) and cultured in RPMI 1640 medium (ATCC modification) containing 10% fetal bovine serum and Antibiotic-Antimycotic from Gibco, Invitrogen (Carlsbad, CA, USA). The cells were cultured at 37 °C with an atmosphere of 5% CO₂.

2.3. Mitochondrial assays

DU-145 cells (2.5×10^4) were seeded per well in XF24 plates and incubated at 37 °C / 5% CO₂ in complete RPMI medium. After 12Hrs complete medium was replaced with nutrient depleted four-day culture media: conditioned media (CM) and incubated for 4 Hrs. Cells were then treated for another 2 Hrs with STAT3 inhibitors prior to analysis using a Seahorse XF24 Analyzer. The Oxygen Consumption Rate (OCR) was measured in DMEM XF base medium containing 10 mM glucose, 2 mM glutamine and 1 mM pyruvate, before and after the sequential injection of oligomycin, FCCP and rotenone/antimycin A, as indicated in (Fig. 1), to final concentrations of 1 µM, 1 µM and 0.5 µM, respectively.

2.4. Cell fractionation

Cells were treated for 16 Hrs with STAT3 inhibitors at a concentration of 10 µM and 1% DMSO in glucose depleted conditioned media (CM), as described [6]. Lysates

were fractionated into cytosol, organelle, nuclei, and cytoskeleton subcellular fractions using ProteoExtract kit (Calbiochem, San Diego, California, USA) according to the manufacturer's directions. Enrichment of each fraction was assessed by SDS-PAGE and immunoblotting using antibodies against GAPDH (cytosol and organelles, Fractions I and II), Histone H2B (nucleus, Fraction III), and Vimentin (cytoskeleton and insoluble proteins, Fraction IV).

2.5. Expression and purification of recombinant STAT3

STAT3 (127–722) cDNA was cloned into a pET15b vector and transformed in BL21 (DE) (Life Technologies, Inc. Woburn, MA, USA). Expression of the recombinant protein was induced by 0.5 mM IPTG, at 20 °C for 5 Hrs. The recombinant STAT3 protein was purified by ammonium sulfate precipitation followed by an ion exchange step with a HiTrap Q column (GE Healthcare Bio-Sciences, Uppsala Sweden) and size exclusion chromatography to achieve purity of over 98%.

2.6. Glutathione reaction studies

STAT3 inhibitors (10 ul of 10 mM stock in DMSO) were spiked into reaction buffer [50 mM HEPES pH7.5 containing 10 mM reduced glutathione (GSH)] the samples were mixed thoroughly and placed in an autosampler set at 20 °C. The reactions were monitored by high performance liquid chromatography (HPLC) using an Exion LC Sciex unit equipped with a UV detector. The stationary phase used was a C18 Synergi™ 4 µm Fusion-RP 80 Å LC column (50 × 2 mm), the mobile phase was water (A) and acetonitrile (B). The elution process consisted of a gradient starting at 20% mobile phase B to 80% for 2 min. The flow rate was maintained at 0.5 mL/min during the run. Measurements were conducted at intervals of 5 min for a period of 50 min total. The presence of the STAT3 inhibitors were quantified by calculating the area under the curves (AUCs) of the compound peaks at 260–295 nm.

2.7. STAT3 alkylation studies

Purified recombinant core fragment of STAT3β protein in ammonium bicarbonate buffer (10 uM) was mixed with each compound at a final concentration of 100 uM. The protein mixture was then incubated at 37 °C overnight. Samples were reduced with 5 mM DTT at 37 °C for one hour and further alkylated with iodoacetamide (15 mM) for 30 min at room temperature in the dark, followed by digestion with trypsin gold in a dry incubator at 37 °C overnight. Formic acid was added the next day to a final concentration of 5% and each protein sample was diluted in 5 mM ammonium acetate containing 0.5% formic acid immediately prior to analysis by targeted mass spectrometry Multiple Reaction Monitoring (MRM).

2.8. Lc-MS/MS

A QTRAP 5500 Sciex hybrid quadrupole-linear ion trap system with a turbo ion spray source coupled to a Sciex LC Exion liquid chromatography system (Redwood City, CA, USA) were used to analyze tryptic digests of STAT3 protein samples treated with STAT3 inhibitors. Fractionation of the samples was done using a Waters Symmetry C18 column

(100 Å, 3.5 µm, 4.6 mm × 150 mm) with a 30 min linear gradient of acetonitrile containing 0.1% formic acid at a flow rate of 300 µL/min. A transition list of cysteine-containing peptides with expected drug-cysteine adducts was generated in Skyline software and exported to the QTRAP mass spectrometer for the development of the acquisition method. Resultant raw data files were imported back into Skyline for analysis and additional processing.

2.9. High resolution LC/MS

Aliquots of the tryptic digests of STAT3 proteins treated with DMSO (control) and those treated with Stattic and TTI-101 were analyzed by LC-MS/MS on an Ultimate 3000 RSLC-Nano chromatograph interfaced to an Orbitrap Fusion high-resolution mass spectrometer (Thermo Scientific, Waltham MA). All MS/MS data were analyzed using Sequest-HT (Thermo Scientific). Proteins were identified by searching their fragment spectra against the Swiss-Prot protein database (EBI). The iodoacetamide derivative of cysteine, stattic adducts of cysteine, and the predicted TTI-101 adducts of cysteine were specified as variable modifications. To access for potential unknown modifications, the data was analyzed in MaxQuant using the dependent peptide search option [12]. An all-peptides output list was analyzed by comparing Stattic, TTI-101 and TTI-101_{ox} with DMSO treated samples, as described in [13].

2.10. Animals

Male and female C57BL/6J mice were purchased from Jackson Laboratories (Bar Harbor, ME) and housed at the University of Texas MD Anderson Cancer Center animal facility (Houston, TX) on a regular 12-hour light/dark cycle with free access to food and water. Mice were group-housed on the same rack in individually ventilated cages. Mice were 8 – 10 weeks of age at the start of the experiment and were randomly assigned to groups (cage) by animal care givers not involved in the experiment. Investigators were blinded to treatment until group data were analyzed and the code was broken by an investigator not involved in the study. All experimental procedures were consistent with the National Institute of Health Guidelines for the Care and Use of Laboratory Animals and the Ethical Issues of the International Association for the Study of Pain [14] and were approved by the Institution for Animal Care and Use Committee (IACUC) of M.D. Anderson Cancer Center. Experiments were performed and reported in compliance with the ARRIVE guidelines [15].

2.11. Pain measurements and chemotherapy-induced peripheral neuropathy (CIPN)

The effect of TTI-101 and chemotherapy on mechanical sensitivity as a read out for pain were assessed over time using von Frey hairs (0.02, 0.07, 0.16, 0.4, 0.6, 1.0, and 1.4 g; Stoelting, (Wood Dale, Illinois, USA) and the up and down method as described previously [16,17]. Cisplatin was diluted in sterile PBS and administered i.p. at a dose of 2.3 mg/kg per day for 5 days followed by 5 days of rest and another 5 days of injections [18]. After 17 days of the last dose of cisplatin the mice were treated with TTI-101 (50 mg/kg i.p. every other day) for a total of seven doses.

2.12. Spared nerve injury (SNI)

SNI surgery was performed on male and female C57BL/6j mice (8 weeks old; Jackson Laboratories), as described [19]. The sural, common peroneal and tibial branches of the sciatic nerve of the left hind paw were exposed under isoflurane anesthesia. A silk suture was used to ligate the common peroneal and tibial branches and 2–4 mm of the distal ends were removed. The sural nerve was left intact. Mice received buprenorphine right before and 1 h after surgery. Mice were treated with 6 doses of TTI-101 (50 mg/kg in vehicle—60% Labrasol/40% PEG-400—or vehicle alone) administered by oral gavage every other day starting on day 10 after SNI. Mechanical sensitivity was monitored over time using von Frey hairs.

2.13. Data and analysis

Studies were designed to include groups of equal size, using randomization and blinded analysis. Statistical analysis was undertaken for studies where each group size was at least $n = 5$, with the exception of the CIPN study where 4 mice per group were used. Animal group size selection for mechanical allodynia was based on previously published data for similar experiments in which sample size calculations were established [19]. Pain behavior data were normally distributed and analyzed by Two-way repeated measures ANOVA followed by Tukey post tests using PRISM8 software; $P < 0.05$ was considered statistically significant. Data from all animals enrolled were included in the final analysis.

2.14. RNA-seq and transcriptome analysis of dorsal root ganglion (DRG)

Whole-genome RNA sequencing was used to identify transcriptional changes induced by cisplatin and TTI-101 in the DRG of 3 mice per group. Total RNA was isolated with the RNeasy MinElute Cleanup Kit (Qiagen, Hilden, Germany). Libraries were prepared with the Stranded mRNA-Seq kit (Kapa Biosystems, Wilmington, MA) following the manufacturer's guidelines. Stranded-mRNA seq was performed with a HiSeq4000 Sequencer (Illumina, San Diego, CA) with 76nt PE format by the RNA Sequencing Core at MD Anderson Cancer Center.

Data analysis was performed as previously described [20,21]. Briefly, expression data of three samples per group were analyzed in R using bioconductor packages. STAR was used for alignment of paired-end reads to the mm10 version of the mouse reference genome; featureCounts was used to assign mapped sequence reads to genomic features, and DESeq2 was used to identify differentially expressed genes ($\text{padj} < 0.05$). Quality check of raw and aligned reads was performed with FastQC and Qualimap. Next, we used Ingenuity Pathway Analysis (IPA; Qiagen Inc., <https://www.qiagenbioinformatics.com/products/ingenuity-pathway-analysis/>) for analysis of the canonical pathways implicated by cisplatin-induced transcriptome changes in DRG.

3. Results

3.1. TTI-101 does not affect mitochondrial function

Mitochondrial dysfunction has been demonstrated to contribute to drug-related SEA [22]. Examination of TTI-101 for safety in 28-day IND-enabling studies in rats and dogs [9], as

well as in a Phase I clinical trial of patients with advanced solid tumors through dose level 4 [11], did not demonstrate any serious toxicity including lactic acidosis, which is a clinical manifestation of mitochondrial dysfunction. However, to determine if TTI-101 caused subclinical abnormalities in mitochondrial function, we examined the effects of TTI-101 and four other direct STAT3 inhibitors on mitochondrial respiration using a Seahorse XF Cell Mito Stress Test kit that measured basal respiration, ATP production, maximal respiration, proton leak, and spare respiratory capacity. The OCR curves of cells incubated with TTI-101 at concentrations 10-fold higher than its IC₅₀ for STAT3 inhibition [9] were similar to cells treated with DMSO control (Fig. 1A–C). Similarly, STA21 and Stattic did not consistently alter the OCR curves compared to DMSO at these concentrations (Fig. 1A–C).

In contrast, marked abnormalities were observed in the OCR curves of cells treated with cryptotanshinone and WP1066 (Fig. 1A, B). Overall, the effects of cryptotanshinone on the OCR curves mimicked a mitochondrial uncoupler, which creates a ‘shot-circuit’ in the oxidative process by inducing a proton leak (PL) such that the loss of proton motive force proceeds without ATP generation. Cells incubated with cryptotanshinone (30 uM) demonstrated a concentration-dependent increase in basal respiratory rate compared to control cells and decreased responses to oligomycin and to antimycin A/rotenone treatment. In addition, cryptotanshinone blocked cell responses to FCCP treatment and resulted in a 50% reduction in ATP level production. (Fig. 1A–C). To further examine the effects of cryptotanshinone on ATP production, we measured the fraction of basal mitochondrial oxygen consumption linked to ATP synthesis (coupling efficiency); coupling efficiency was significantly reduced (Fig. 1C), further indicative of mitochondrial dysfunction. In addition, the OCR after oligomycin treatment, which is a direct measure of the proton leak rate (Fig. 1C), showed a significant increase in proton leak in cells incubated with cryptotanshinone (30 uM) indicating that mitochondria are uncoupled and severely damaged [23,24]. Similar to cryptotanshinone, we observed marked abnormalities in the OCR curves of cells treated with WP1066. (Fig. 1A–C) indicative of mitochondrial dysfunction [24], including diminished basal OCR, ATP production rate, maximal respiration, spare respiratory capacity, and coupling efficiency.

3.2. TTI-101 does not induce STAT3 aggregation in cells

STAT3 inhibitors that were demonstrated to impair mitochondrial activity also were found to cause STAT3 to aggregate in cells under low glucose conditions [6]. Using similar experimental conditions, we assessed the effects of TTI-101 and other direct STAT3 inhibitors on the partitioning and oligomeric state of STAT3. Cells were incubated in medium containing each STAT3 inhibitor at 10 uM final concentration for 16 h. Cells were fractionated and fractions I through IV were separated by SDS-PAGE and immunoblotted using antibodies selective for each fraction (Fig. 2). TTI-101 had no effect on the intracellular localization of STAT3; similar results were obtained in cells incubated with STA21 and Stattic. In contrast, in cells treated with cryptotanshinone or WP1066, over half of STAT3 was found in the insoluble fraction (Fraction IV) indicating that each induced formation of STAT3 intracellular aggregates, which explains their adverse effects on mitochondrial function and confirms the findings of Genini et.al. [6].

3.3. TTI-101 does not react with GSH or covalently modify STAT3

Surface Plasmon Resonance (SPR) studies that directly examined the ability of TTI-101 to inhibit STAT3 binding to its immobilized pY-peptide ligand were performed under reducing conditions [9,25]. Furthermore, the shape of the binding inhibition curves was most consistent with competitive inhibition. However, intracellular protein depletion through aggregation has recently been described as a key mechanism of action of compounds, such as DUB Inhibitors b-AP15 and VLX1570 that possess α,β -unsaturated carbonyl moieties capable of covalently reacting with their target [26]. Soon after its discovery, Stattic was proposed to alkylate STAT3 via a Michael addition reaction at C687 located within the SH2 domain, but outside the pY-peptide binding pocket; this alkylation event was proposed to allosterically alter the structure of the pY-peptide binding pocket interfering with its ability to bind ligand [27]. More recently, SI3-201 and related compounds were shown to modify STAT3 in a manner consistent with thiolmediated *O*-tosyl substitution [28].

We performed two studies to determine directly if TTI-101 mediates its inhibitory effect on STAT3 through covalent modification. The first study was a UV-HPLC-based assay to determine the stability of TTI-101, as well as the other STAT3 inhibitors, in the presence of a natural nucleophile—reduced glutathione (GSH). TTI-101 and the other inhibitors were reconstituted at 100 μ M in 50 mM HEPES buffer at pH 7.5 containing 10 mM GSH. Each reaction mixture was sampled at time 0 and every 5 min for 50 min; all samples were analyzed by HPLC. The amount of unreacted inhibitor was determined by measuring the area under the curve (AUC) and plotting this value as a percentage of the starting AUC as a function of time (Fig. 3). Consistent with early reports of it serving as a Michael's acceptor, Stattic levels decreased rapidly within 5 min to < 10% of baseline in the presence of GSH while remaining constant in the absence of GSH (Fig. 3). In contrast, there was no loss of TTI-101 in the presence of GSH up to 50 min after exposure; similar results were observed for cryptotanshinone, WP1066 and STA21.

Review of the structure of TTI-101 did not reveal a potential mechanism for alkylation of STAT3 by a Michael addition or by thiolmediated *O*-tosyl substitution. However, enol-to-ketone oxidation within the first hydroxy-naphthalene group of TTI-101 would form TTI-101_{OX} (Fig. 4), which potentially could undergo a Michael addition reaction. To examine this possibility, we generated recombinant STAT3 post-translationally unmodified in bacteria using a cDNA construct in which the domain containing the N-terminal oligomerization domain was deleted (STAT3 β tr); this domain is not necessary for native folding of the core domains of STAT3 (CCD, DBD, linker domain, and SH2 domain) and its removal markedly improves recombinant STAT3 protein solubility. STAT3 β tr contains 11 Cys residues. To determine how many of these Cys residues are available to be alkylated when the soluble protein is natively folded, we incubated STAT3 β tr with two protein alkylating agents, iodoacetamide and N-ethylmaleimide (NEM) under conditions optimal for alkylation (Fig. 4A). Using data obtained on a quadrupole-linear ion trap MS (Sciex QTrap 5500), we detected adducts based on the presence of predicted MRM signal for peptides containing cysteine residues. The identity of the peptides were confirmed by performing full MS/MS spectra on the detected transitions. The LC-MS/MS of the tryptic digested protein

revealed 6 peptides alkylated by iodoacetamide and NEM. Five of the peptides contained a single alkylated Cys, while one of the peptides contained two alkylated Cys residues.

We next performed targeted and untargeted LC-MS/MS analysis using a QTrap 5500 and an Orbitrap-Ellite mass spectrometer on tryptic digests of STAT3 β tr incubated with TTI-101 or Stattic under optimal alkylating conditions. If TTI-101 or TTI-101_{OX} alkylated STAT3, we would expect a shift in the mass of peptides containing Cys residues by the equivalent of the exact mass of TTI-101_{ox} as TTI-101 needs to undergo oxidation at the -OH located para to the sulfonamide group to form a Michael's acceptor. We were unable to detect adducts of TTI-101 or TTI-101_{ox} on Cys containing peptides by targeted LC-MS/MS (Fig. 4C). To ensure that the failure to detect alkylated protein incubated with TTI-101 was not due to insufficient generation of oxidized TTI-101 under the experimental conditions, we synthesized TTI-101_{OX} itself and incubated it with STAT3 β tr. Similar to results obtained with TTI-101, no alkylated peptides were detected upon incubation with TTI-101_{OX} indicating that STAT3 is not alkylated by TTI-101 in either its reduced or oxidized form. In contrast to TTI-101, tryptic digests of STAT3 β tr incubated with Stattic under similar conditions demonstrated that Stattic efficiently alkylated STAT3 at seven sites (Fig. 5A–C).

We then evaluated the possibility that TTI-101—reduced or oxidized—may covalently modify STAT3 and result in a mass shift on LC-MS/MS that is not detectable using the targeted detection approach described above. We performed high resolution LC-MS/MS analysis of protein digests after incubation of STAT3 with TTI-101 or TTI-101_{OX} using an Orbitrap-Ellite mass spectrometer and analyzed the data using an approach described by Antinori et. al that is tailored for the detection of unknown chemical adduct modifications on proteins [13]. Using this approach, we were able to detect Stattic adducts in protein digests of STAT3 incubated with Stattic. However, we did not identify adducts in digests of STAT3 incubated with either TTI-101 or TTI-101_{OX}, confirming that neither forms of TTI-101 covalently modify STAT3 (Fig. 5D).

3.4. TTI-101 suppresses chemotherapy-induced mechanical allodynia

Peripheral neuropathy has been observed with several small-molecule STAT3 inhibitors in clinical-stage development [4–6]. To assess whether TTI-101 causes peripheral neuropathy, male C57BL/6 mice were treated with 7 doses of TTI-101 (50 mg/kg i.p. every other day) and sensitivity to mechanical stimulation was followed over time using von Frey hairs. Administration of TTI-101 alone had no effect on mechanical sensitivity (Fig. 6A). To investigate whether TTI-101 aggravates existing neuropathic pain, we used the cisplatin model of chemotherapy-induced peripheral neuropathy (CIPN). This model was selected because we showed previously that it is mediated by mitochondrial damage in the peripheral nervous system [17,29]. Mice were treated with two cycles of cisplatin (5 daily doses of 2.3 mg/kg followed by 5 days rest), which induces mechanical allodynia (Fig. 6B) that lasts for at least 75 days [17]. TTI-101 administration (50 mg/kg i.p. every other day for a total of 7 doses) was started 17 days after the last dose of cisplatin, when mechanical allodynia had developed fully. TTI-101 administration markedly reduced cisplatin-induced mechanical allodynia (Fig. 6B). The beneficial effect of TTI-101 developed slowly over time—maximal

inhibition was obtained after the 4th dose of TTI-101 and was maintained while dosing continued. Mechanical allodynia returned to levels similar to those in mice treated with cisplatin alone 4 days after the last dose of TTI-101.

3.5. TTI-101 suppresses SNI-induced mechanical allodynia

To determine whether the beneficial effect of TTI-101 is limited to CIPN or is more broadly applicable to other causes of neuropathic pain, we examined its effect on mechanical allodynia induced by SNI. SNI induces profound mechanical allodynia in male and female mice. Administration of TTI-101 in the SNI model reduced mechanical allodynia within 6 h of the first dose (Fig. 7A) and repeated dosing of TTI-101 over 14 days led to complete reversal of SNI-induced mechanical allodynia in male and female mice (Fig. 7B) that was sustained through day 52 of the experiment or 40 days after the last dose of TTI-101.

3.6. RNA-seq analysis of effect of TTI-101 on the DRG transcriptome in cisplatin-treated mice

To determine whether the beneficial effect of TTI-101 on CIPN is associated with changes in the transcriptome and, in particular, in expression of STAT3 target genes, we performed RNA-seq analysis on dorsal root ganglia (DRG). Mice were treated with cisplatin followed by TTI-101 as in Fig. 6 and lumbar DRG were collected at 4 Hrs after the fourth dose of TTI-101 or vehicle. Comparison of the transcriptome in DRG from mice treated with cisplatin vs. PBS showed that cisplatin changed the expression of 1,973 genes (675 down, 1,298 up; Fig. 8A). TTI-101 administration to cisplatin-treated mice changed expression of 1,713 genes (1,416 down, 297 up) vs. mice treated with cisplatin alone. Notably, the 443 genes that were altered in both groups (PBS vs. Cis and Cis vs. Cis + TTI-101) showed an overall opposite expression pattern between groups, indicating that TTI-101 administration normalized the expression of genes whose expression was altered in cisplatin-treated mice (Fig. 8B and Table 1).

Ingenuity pathway analysis (IPA) focused on canonical pathways (Fig. 8C) and showed that the 443 genes were mainly associated with neuronal health and survival pathways (namely synaptogenesis signaling pathways, TNFR signaling, axonal guidance signaling, Semaphorin Signaling in Neurons, Ephrin signaling). Upstream regulator analysis of the 1,713 differentially expressed genes (DEG) that changed with TTI-101 administration revealed huntingtin (HTT), amyloid beta precursor protein (APP), TP53, TGF β 1, and estrogen receptor as the top five upstream regulators driving downstream changes (Table 2). The mechanistic network of four regulators identified STAT3 as an intermediate regulator. Consistent with the activity of TTI-101 as a STAT3 inhibitor, STAT3 activity was reduced in all networks (Fig. 8D). For example, for the TP53 network, 14 regulators were part of the mechanistic network which together influence expression of 481 genes and out of these 481 genes, 64 target genes are regulated by STAT3.

To gain further insight into potential mechanisms underlying TTI-101's reversal of CIPN, we used IPA to perform a comparison analysis (Fig. 9A). IPA identified VEGF as the top upstream regulator different between the groups—PBS vs. Cis and Cis vs. Cis + TTI-101. Specifically, IPA predicted activation of VEGF signaling in mice treated with cisplatin

as compared to PBS. This pathway was inhibited when cisplatin-treated mice received TTI-101. The heat map in Fig. 9B shows the effect of TTI-101 administration on the target genes in VEGF signaling network.

4. Discussion

Small-molecule inhibitors that target the SH2 domain of STAT3 have been proposed recently as an example of synthetic lethality; upon STAT3 binding, they induce formation of proteotoxic aggregates that inhibit mitochondrial function leading to cell death, especially in cancer cells experiencing metabolic stress [6]. Perhaps, not surprisingly, cancer patients enrolled in Phase I/II clinical studies of some drugs within this class have experienced SAE, such as lactic acidosis and peripheral neuropathy, which are clinical manifestations of mitochondrial toxicity; these SAE have halted further patient enrollment. Our group developed TTI-101, a competitive inhibitor of STAT3 designed to target the pY-peptide binding site within STAT3's SH2 domain and to directly block two key steps in its activation—recruitment to activated cytokine receptor complexes and homodimerization. The studies reported here were undertaken to determine if TTI-101 targets STAT3's mitochondrial function, causes STAT3 aggregation, or induces peripheral neuropathy. We report that TTI-101 does not affect mitochondrial function, does not cause STAT3 aggregation through chemical modification or other means, and does not induce pain measured as mechanical allodynia. In fact, TTI-101 administration unexpectedly suppressed mechanical allodynia induced by the chemotherapeutic agent cisplatin, indicating it may be of special benefit when administered to cancer patients at risk of developing chemotherapy-induced peripheral neuropathy (CIPN).

While the Otsuka compounds were unavailable to us for study, we examined two compounds (WP1066 and cryptotanshinone) previously demonstrated to markedly affect mitochondrial function for evidence of covalent modification of STAT3, in particular, alkylation. LC-MS/MS of STAT3 protein incubated with WP1066 and cryptotanshinone revealed no alkylation at cysteine sites. In contrast, Stattic, which did not affect mitochondrial function, alkylated STAT3 at all detectable cysteines. STA21, which emerged from a virtual ligand screen for compounds that bind the STAT3 SH2 domain [30], behaved in manner identical to TTI-101; it neither alkylated STAT3 nor induced mitochondrial toxicity. Thus, the ability of STAT3 inhibitors to cause STAT3 aggregation and mitochondrial toxicity is not related to their ability to covalently modify STAT3 and their precise mechanism for inducing STAT3 aggregation remains uncertain.

We previously demonstrated that administration of TTI-101 to rats for 28 days (up to a dose of 200 mg/kg/day) and to dogs (up to a dose of 100 mg/kg/day) did not cause any metabolic abnormalities including lactic acidosis. Increasing evidence indicates that, in addition to lactic acidosis, mitochondrial dysfunction plays a key role in the development of chemotherapy-induced neuropathic pain [31–33]. Peripheral neuropathy is one of the SAE that have been observed with some small-molecule STAT3 inhibitors in clinical-stage development [5]. Our current findings show that treatment of naïve mice with TTI-101 does not induce neuropathic pain in the von Frey test of mechanical allodynia (Fig. 6A), which is commonly used to assess for peripheral neuropathic pain in rodent models.

It is conceivable that potential additional damage to mitochondria as a result of STAT3 inhibition would aggravate CIPN. However, our data demonstrated that TTI-101 treatment had the opposite effect; administration of TTI-101 suppressed established mechanical allodynia in mice treated with cisplatin. Preliminary data also indicated that TTI-101 suppressed existing mechanical allodynia in mice treated with paclitaxel or docetaxel, two chemotherapeutics of a different class. In addition, TTI-101 markedly reduced mechanical allodynia in the SNI model. SNI increases levels of pY-STAT3 in spinal cord astrocytes [34]. In addition, there is evidence for increased pY-STAT3 in microglia in the spinal cord in the spinal nerve injury model of neuropathic pain in rats [35]. While intrathecal administration of the Janus kinase 2 inhibitor, AG490, attenuated mechanical allodynia in both models [36], there are no published reports describing the effects of a STAT3 inhibitor on mechanical allodynia in response to SNI. Transgenic expression of constitutively active and dominant-negative forms of STAT3 in astrocytes located within the spinal dorsal horn (SDH) of mice and rats showed that activation of astrocytic STAT3 plays an important role in maintaining neuropathic pain [37]. Two previous studies reported the beneficial effect of STAT3 inhibitor treatment on chemotherapy-induced neuropathy; administration of the STAT3 inhibitor S3I-201 to rats during treatment with oxaliplatin, paclitaxel, or vincristine reduced mechanical allodynia [38,39]. However, the reduction in mechanical allodynia was only partial, and S3I-201 was administered intrathecally. Our data indicate that mechanical allodynia is reduced to baseline levels in response to oral administration of TTI-101, making this a more attractive compound for clinical application. It remains to be determined whether co-administration of TTI-101 with cisplatin will fully or partially prevent development of CIPN.

The beneficial effect of the STAT3 inhibitor S3I-201 in CIPN cited above was associated with normalization of the expression of CXCL12 a chemokine that was shown to be upregulated in the DRG of rats or mice treated with oxaliplatin, vincristine or paclitaxel. In our RNA-seq data set, we did not detect significant changes in CXCL12, although there was a trend towards increased levels (\log_2FC 0.176) in response to cisplatin and a trend towards reduced levels (\log_2FC - 0.474) in response to administration of TTI-101 in cisplatin-treated mice. In addition, our RNA-seq analysis of the DRG transcriptome indicated that TTI-101 administration to cisplatin-treated mice normalizes expression of 443 out of the 1,973 genes (22 %) that were changed in response to cisplatin treatment. These genes are mainly associated with neuronal health and survival pathways, indicating that TTI-101 also may help to restore the loss in intra-epidermal nerve fiber density that is associated with CIPN. We also saw enrichment in genes related to the TNFR1 pathway after TTI-101 administration. This may indicate inhibition of TNF signaling, which has been shown to reduce STAT3 activation. In oxaliplatin-mediated neuropathy, administration of a neutralizing antibody against TNF- α prevented STAT3 activation in DRG [38].

To get additional insight into the potential mechanism underlying the suppression of cisplatin-induced mechanical allodynia, we used the IPA comparison analysis tool to identify upstream regulators of the pathways that were altered in response to cisplatin and reversed by administration of TTI-101. The STAT3 target VEGF [40,41] was identified as the top upstream regulator. It has been shown that activation of retinal neuronal STAT3 increases neuronal VEGF production [42]. In addition, DRG expression of *Flt1*, the gene

encoding the VEGF receptor 1 (VEGF-R1), was upregulated in response to cisplatin (log₂FC 0.295) and this was reversed by administration of TTI-101 (log₂FC – 0.503). We also found the VEGF-associated downstream kinase, PI3K, was downregulated by TTI-101 (log₂FC – 0.408). Interestingly, it has been shown that VEGF signaling to VEGFR1 on sensory neurons promotes pain in models of cancer pain [43]. Moreover, administration of an anti-VEGF antibody attenuated oxaliplatin-induced mechanical allodynia [44]. In addition, treatment with a PI3K inhibitor attenuated mechanical allodynia induced by VEGFA in mice. In contrast, however, there also is evidence for aggravation of chemotherapy-induced neuropathies by co-administration of anti-VEGF antibodies in patients and mice [45,46]. Further studies are needed to address the potential role of changes in local VEGF signaling in the DRG in the beneficial effect of TTI-101 on cisplatin-induced peripheral neuropathy.

We previously demonstrated that mitochondrial damage contributes to neuropathic pain [17,29]. STAT3 signaling is essential for mitochondrial function; consequently, reports of peripheral neuropathy as an SAE in clinical trials of STAT3 inhibitors that impair mitochondrial function were not totally unexpected. Here, we show that TTI-101, a competitive inhibitor STAT3, did not affect mitochondrial function and not only did not cause peripheral neuropathy, rather, it markedly reduced cisplatin-induced mechanical allodynia through modulating several signaling networks linked to CIPN. Thus, TTI-101 may be an attractive agent for cancer treatment, especially in combination with chemotherapy agents that cause CIPN.

Acknowledgments

We thank the Mouse Metabolism and Phenotyping Core Facility at Baylor college of Medicine and the UT MD Anderson Proteomics and Metabolomics Facility, which is generously supported by the MD Anderson Cancer Center NIH High-End Instrumentation program grant 1S10OD012304-01 and CPRIT Core Facility Grant RP130397. These studies also were supported by NIH grants RO1DK114356 and UM1HG006348 and endowment funds from the University of Texas MD Anderson Cancer Center.

References

- [1]. Bharadwaj U, Kasembeli MM, Robinson P, Tweardy DJ, Targeting janus kinases and signal transducer and activator of transcription 3 to treat inflammation, fibrosis, and cancer: rationale, progress, and caution, *Pharmacol. Rev.* 72 (2) (2020) 486–526. [PubMed: 32198236]
- [2]. Kasembeli M, Bharadwaj U, Robinson P, Tweardy D, Contribution of STAT3 to inflammatory and fibrotic diseases and prospects for its targeting for treatment, *Int. J. Mol. Sci.* 19 (8) (2018) 2299, 10.3390/ijms19082299.
- [3]. Dang CV, Reddy EP, Shokat KM, Soucek L, Drugging the ‘undruggable’ cancer targets, *Nat. Rev. Cancer* 17 (8) (2017) 502–508. [PubMed: 28643779]
- [4]. Bendell JC, Hong DS, Burris HA, Naing A, Jones SF, Falchook G, Bricmont P, Elekes A, Rock EP, Kurzrock R, Phase 1, open-label, dose-escalation, and pharmacokinetic study of STAT3 inhibitor OPB-31121 in subjects with advanced solid tumors, *Cancer Chemother. Pharmacol.* 74 (1) (2014) 125–130. [PubMed: 24819685]
- [5]. Ogura M, Uchida T, Terui Y, Hayakawa F, Kobayashi Y, Taniwaki M, Takamatsu Y, Naoe T, Tobinai K, Munakata W, Yamauchi T, Kageyama A, Yuasa M, Motoyama M, Tsunoda T, Hatake K, Phase I study of OPB-51602, an oral inhibitor of signal transducer and activator of transcription 3, in patients with relapsed/refractory hematological malignancies, *Cancer Sci.* 106 (7) (2015) 896–901. [PubMed: 25912076]

- [6]. Genini D, Brambilla L, Laurini E, Merulla J, Civenni G, Pandit S, D'Antuono R, Perez L, Levy DE, Pricl S, Carbone GM, Catapano CV, Mitochondrial dysfunction induced by a SH2 domain-targeting STAT3 inhibitor leads to metabolic synthetic lethality in cancer cells, *PNAS* 114 (25) (2017) E4924–E4933. [PubMed: 28584133]
- [7]. Garama DJ, Harris TJ, White CL, Rossello FJ, Abdul-Hay M, Gough DJ, Levy DE, A Synthetic Lethal Interaction between Glutathione Synthesis and Mitochondrial Reactive Oxygen Species Provides a Tumor-Specific Vulnerability Dependent on STAT3, *Mol. Cell. Biol.* 35 (21) (2015) 3646–3656. [PubMed: 26283727]
- [8]. Yang R, Rincon M, Mitochondrial Stat3, the Need for Design Thinking, *International journal of biological sciences* 12 (5) (2016) 532–544. [PubMed: 27019635]
- [9]. Bharadwaj U, Eckols TK, Xu X, Kasembeli MM, Chen Y, Adachi M, Song Y, Mo Q, Lai SY, Tweardy DJ, Small-molecule inhibition of STAT3 in radioresistant head and neck squamous cell carcinoma, *Oncotarget* 7 (18) (2016) 26307–26330. [PubMed: 27027445]
- [10]. Bharadwaj U, Kasembeli MM, Tweardy DJ, STAT3 Inhibitors in Cancer: A Comprehensive Update, in: Ward AC (Ed.), *STAT Inhibitors in Cancer*, Springer International Publishing, Cham, 2016, pp. 95–161.
- [11]. [NCT03195699](https://ClinicalTrials.gov/show/NCT03195699), Oral STAT3 Inhibitor, TTI-101, in Patients With Advanced Cancers, June 22, 2017. <https://ClinicalTrials.gov/show/NCT03195699>.
- [12]. Tyanova S, Temu T, Cox J, The MaxQuant computational platform for mass spectrometry-based shotgun proteomics, *Nat. Protoc.* 11 (12) (2016) 2301–2319. [PubMed: 27809316]
- [13]. Antinori P, Michelot T, Lescuyer P, Müller M, Acosta-Martin AE, Detection of Unknown Chemical Adduct Modifications on Proteins: From Wet to Dry Laboratory, in: Evans CA, Wright PC, Noirel J (Eds.), *Mass Spectrometry of Proteins: Methods and Protocols*, Springer, New York, NY, 2019, pp. 99–113.
- [14]. Zimmermann M, Ethical guidelines for investigations of experimental pain in conscious animals, *Pain* 16 (2) (1983) 109–110. [PubMed: 6877845]
- [15]. Kilkenny C, Browne WJ, Cuthill IC, Emerson M, Altman DG, Improving bioscience research reporting: the ARRIVE guidelines for reporting animal research, *PLoS Biol.* 8 (6) (2010) e1000412.
- [16]. Chaplan SR, Bach FW, Pogrel JW, Chung JM, Yaksh TL, Quantitative assessment of tactile allodynia in the rat paw, *J. Neurosci. Methods* 53 (1) (1994) 55–63. [PubMed: 7990513]
- [17]. Krukowski K, Ma J, Golonzhka O, Laumet GO, Gutti T, van Duzer JH, Mazitschek R, Jarpe MB, Heijnen CJ, Kavelaars A, HDAC6 inhibition effectively reverses chemotherapy-induced peripheral neuropathy, *Pain* 158 (6) (2017) 1126–1137. [PubMed: 28267067]
- [18]. Mao-Ying Q-L, Kavelaars A, Krukowski K, Huo X-J, Zhou W, Price TJ, Cleeland C, Heijnen CJ, McKemy DD, The anti-diabetic drug metformin protects against chemotherapy-induced peripheral neuropathy in a mouse model, *PLoS ONE* 9 (6) (2014) e100701.
- [19]. Singhmar P, Trinh RTP, Ma J, XiaoJiao Huo, Peng B.o., Heijnen CJ, Kavelaars A, The fibroblast-derived protein PI16 controls neuropathic pain, *PNAS* 117 (10) (2020) 5463–5471. [PubMed: 32079726]
- [20]. Chiu GS, Boukelmoune N, Chiang ACA, Peng B.o, Rao V, Kingsley C, Liu H-L, Kavelaars A, Kesler SR, Heijnen CJ, Nasal administration of mesenchymal stem cells restores cisplatin-induced cognitive impairment and brain damage in mice, *Oncotarget* 9 (85) (2018) 35581–35597. [PubMed: 30473752]
- [21]. Ma J, Trinh RT, Mahant ID, Peng B.o., Matthias P, Heijnen CJ, Kavelaars A, Cell-specific role of histone deacetylase 6 in chemotherapy-induced mechanical allodynia and loss of intraepidermal nerve fibers, *Pain* 160 (12) (2019) 2877–2890. [PubMed: 31356453]
- [22]. Dykens JA, Will Y, The significance of mitochondrial toxicity testing in drug development, *Drug Discovery Today* 12 (17–18) (2007) 777–785. [PubMed: 17826691]
- [23]. Amireddy N, Puttapaka SN, Vinnakota RL, Ravuri HG, Thonda S, Kalivendi SV, The unintended mitochondrial uncoupling effects of the FDA-approved anti-helminth drug nitazoxanide mitigates experimental parkinsonism in mice, *J. Biol. Chem.* 292 (38) (2017) 15731–15743. [PubMed: 28798236]

- [24]. Brand MD, Nicholls DG, Assessing mitochondrial dysfunction in cells, *Biochem. J.* 435 (2) (2011) 297–312. [PubMed: 21726199]
- [25]. Xu X, Kasembeli MM, Jiang X, Tweardy BJ, Tweardy DJ, Schmidt HHHW, Chemical probes that competitively and selectively inhibit Stat3 activation, *PLoS ONE*4 (3) (2009) e4783.
- [26]. Ward JA, Pinto-Fernandez A, Cornelissen L, Bonham S, Diaz-Saez L, Riant O, Huber KVM, Kessler BM, Feron O, Tate EW, Re-evaluating the mechanism of action of alpha, beta-unsaturated carbonyl DUB inhibitors b-AP15 and VLX1570: A paradigmatic example of unspecific protein cross-linking with michael acceptor motif-containing drugs, *J. Med. Chem.* (2020).
- [27]. McMurray JS, A new small-molecule Stat3 inhibitor, *Chem. Biol.* 13 (11) (2006) 1123–1124. [PubMed: 17113993]
- [28]. Ball DP, Lewis AM, Williams D, Resetca D, Wilson DJ, Gunning PT, Signal transducer and activator of transcription 3 (STAT3) inhibitor, S3I-201, acts as a potent and non-selective alkylating agent, *Oncotarget*7 (15) (2016) 20669–20679. [PubMed: 26942696]
- [29]. Maj MA, Ma J, Krukowski KN, Kavelaars A, Heijnen CJ, Inhibition of mitochondrial p53 accumulation by PFT- μ prevents cisplatin-induced peripheral neuropathy, *Front. Mol. Neurosci.* 10 (2017) 108. [PubMed: 28458631]
- [30]. Song H, Wang R, Wang S, Lin J, A low-molecular-weight compound discovered through virtual database screening inhibits Stat3 function in breast cancer cells, *Proceedings of the National Academy of Sciences of the United States of America*102(13) (2005) 4700. [PubMed: 15781862]
- [31]. Bennett GJ, Doyle T, Salvemini D, Mitotoxicity in distal symmetrical sensory peripheral neuropathies. *Nature reviews, Neurology*10 (6) (2014) 326–336. [PubMed: 24840972]
- [32]. Colvin LA, Chemotherapy-induced peripheral neuropathy: where are we now? *Pain*160 Suppl 1 (Suppl 1) (2019) S1–S10. [PubMed: 31008843]
- [33]. Ma J, Kavelaars A, Dougherty PM, Heijnen CJ, Beyond symptomatic relief for chemotherapy-induced peripheral neuropathy: Targeting the source, *Cancer*124 (11) (2018) 2289–2298. [PubMed: 29461625]
- [34]. Liu S, Mi WL, Li Q, Zhang MT, Han P, Hu S, Mao-Ying QL, Wang YQ, Spinal IL-33/ST2 Signaling Contributes to Neuropathic Pain via Neuronal CaMKII-CREB and Astroglial JAK2-STAT3 Cascades in Mice, *Anesthesiology*123 (5) (2015) 1154–1169. [PubMed: 26352378]
- [35]. Dominguez E, Rivat C, Pommier B, Mauborgne A, Pohl M, JAK/STAT3 pathway is activated in spinal cord microglia after peripheral nerve injury and contributes to neuropathic pain development in rat, *J. Neurochem.* 107 (1) (2008) 50–60. [PubMed: 18636982]
- [36]. Tsuda M, Kohro Y, Yano T, Tsujikawa T, Kitano J, Tozaki-Saitoh H, Koyanagi S, Ohdo S, Ji RR, Salter MW, Inoue K, JAK-STAT3 pathway regulates spinal astrocyte proliferation and neuropathic pain maintenance in rats, *Brain*134 (Pt 4) (2011) 1127–1139. [PubMed: 21371995]
- [37]. Kohro Y, Sakaguchi E, Tashima R, Tozaki-Saitoh H, Okano H, Inoue K, Tsuda M, A new minimally-invasive method for microinjection into the mouse spinal dorsal horn, *Sci. Rep.* 5 (2015) 14306. [PubMed: 26387932]
- [38]. Li YY, Li H, Liu ZL, Li Q, Qiu HW, Zeng LJ, Yang W, Zhang XZ, Li ZY, Activation of STAT3-mediated CXCL12 up-regulation in the dorsal root ganglion contributes to oxaliplatin-induced chronic pain, *Molecular pain*13 (2017) 1744806917747425.
- [39]. Xu T, Zhang X-L, Ou-Yang H-D, Li Z-Y, Liu C-C, Huang Z-Z, Xu J, Wei J-Y, Nie B-L, Ma C, Wu S-L, Xin W-J, Epigenetic upregulation of CXCL12 expression mediates antitubulin chemotherapeutics-induced neuropathic pain, *Pain*158 (4) (2017) 637–648. [PubMed: 28072604]
- [40]. Wei D, Le X, Zheng L, Wang L, Frey JA, Gao AC, Peng Z, Huang S, Xiong HQ, Abbruzzese JL, Xie K, Stat3 activation regulates the expression of vascular endothelial growth factor and human pancreatic cancer angiogenesis and metastasis, *Oncogene*22 (3) (2003) 319–329. [PubMed: 12545153]
- [41]. Niu G, Wright KL, Huang M, Song L, Haura E, Turkson J, Zhang S, Wang T, Sinibaldi D, Coppola D, Heller R, Ellis LM, Karras J, Bromberg J, Pardoll D, Jove R, Yu H, Constitutive Stat3 activity up-regulates VEGF expression and tumor angiogenesis, *Oncogene*21 (13) (2002) 2000–2008. [PubMed: 11960372]

- [42]. Sun Y, Ju M, Lin Z, Fredrick TW, Evans LP, Tian KT, Saba NJ, Morss PC, Pu WT, Chen J, Stahl A, Joyal JS, Smith LE, SOCS3 in retinal neurons and glial cells suppresses VEGF signaling to prevent pathological neovascular growth, *Science signaling*8(395) (2015) ra94.
- [43]. Selvaraj D, Gangadharan V, Michalski C, Kurejova M, Stösser S, Srivastava K, Schweizerhof M, Waltenberger J, Ferrara N, Heppenstall P, Shibuya M, Augustin H, Kuner R, A functional role for VEGFR1 expressed in peripheral sensory neurons in cancer pain, *Cancer Cell*27 (6) (2015) 780–796. [PubMed: 26058077]
- [44]. Di Cesare Mannelli L, Tenci B, Micheli L, Vona A, Corti F, Zanardelli M, Lapucci A, Clemente AM, Failli P, Ghelardini C, Adipose-derived stem cells decrease pain in a rat model of oxaliplatin-induced neuropathy: Role of VEGF-A modulation, *Neuropharmacology*131 (2018) 166–175. [PubMed: 29241656]
- [45]. Giantonio BJ, Catalano PJ, Meropol NJ, O'Dwyer PJ, Mitchell EP, Alberts SR, Schwartz MA, Benson AB 3rd, Bevacizumab in combination with oxaliplatin, fluorouracil, and leucovorin (FOLFOX4) for previously treated metastatic colorectal cancer: results from the Eastern Cooperative Oncology Group Study E3200, *J. Clin. Oncol.* 25 (12) (2007) 1539–1544. [PubMed: 17442997]
- [46]. Verheyen A, Peeraer E, Nuydens R, Dhondt J, Poesen K, Pintelon I, Daniels A, Timmermans JP, Meert T, Carmeliet P, Lambrechts D, Systemic anti-vascular endothelial growth factor therapies induce a painful sensory neuropathy, *Brain*135 (Pt 9) (2012) 2629–2641. [PubMed: 22734125]
- [47]. Brademan DR, Riley NM, Kwiecien NW, Coon JJ, Interactive peptide spectral annotator: A versatile web-based tool for proteomic applications, *Mol. Cell. Proteom.* MCP18 (8) (2019) S193–S201.

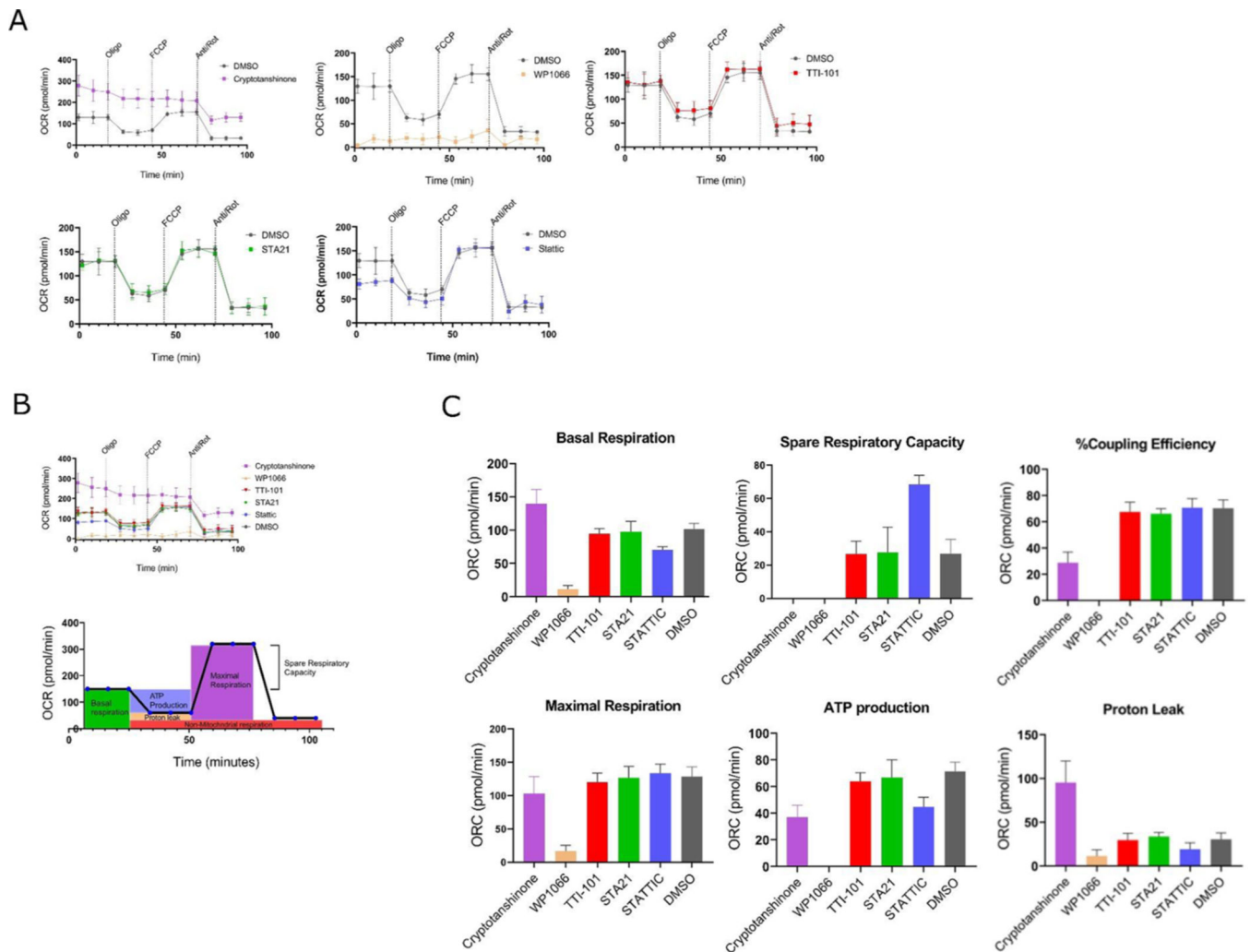


Fig. 1. Effects of STAT3 inhibitors on mitochondrial function. DU-145 cells were treated with the indicated STAT3 inhibitors at 30 μ M for 2 Hrs. Seahorse experiments showing oxygen consumption rate (OCR) by DU-145 cells treated with DMSO alone or DMSO containing the indicated STAT3 inhibitor at 30 μ M prior to and following addition of oligomycin, FCCP, and antimycin A/rotenone, as indicated ($n = 6$). Data in (Fig. 1 A) combined into one graph, showing all the OCR curves relative to each other. Below, figure representing estimation of OCR parameters in(C) Mean \pm SEM of basal respiration, maximal respiration, spare respiratory capacity, ATP production, coupling efficiency and proton leak ($n = 6$).

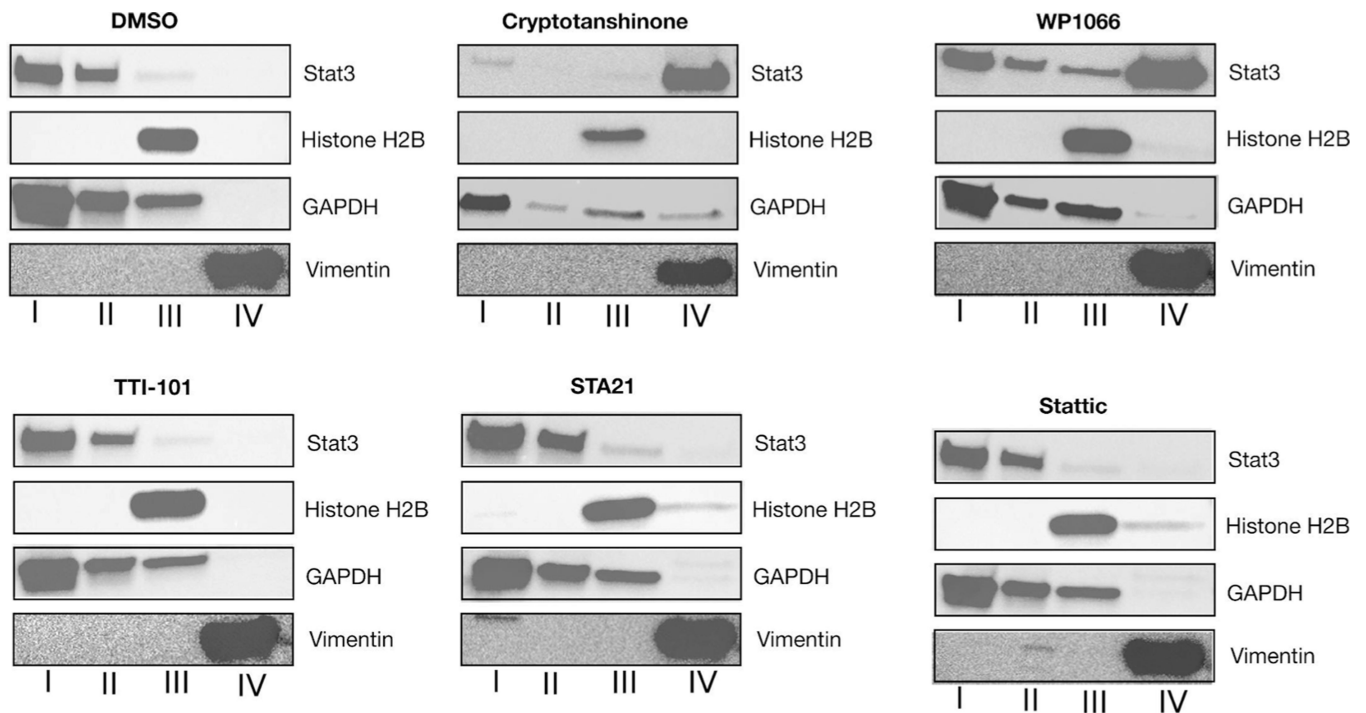


Fig. 2. Immunoblotting of fractions of DU-145 cells incubated with indicated drugs (10uM concentration for 16 Hrs). Fractions were separated using 4–20 % SDS-PAGE and immunoblotted using antibodies against STAT3, Histone H2B, GAPDH and Vimentin. Data are representative of three independently performed experiments.

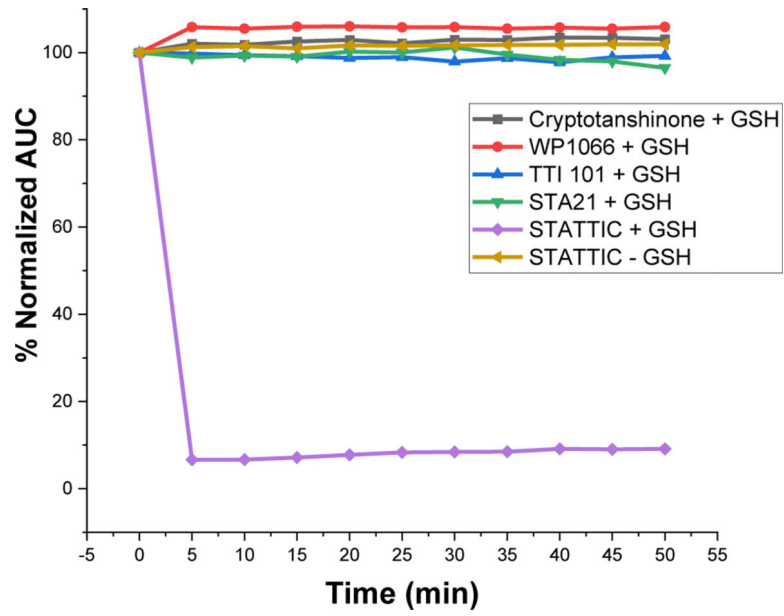
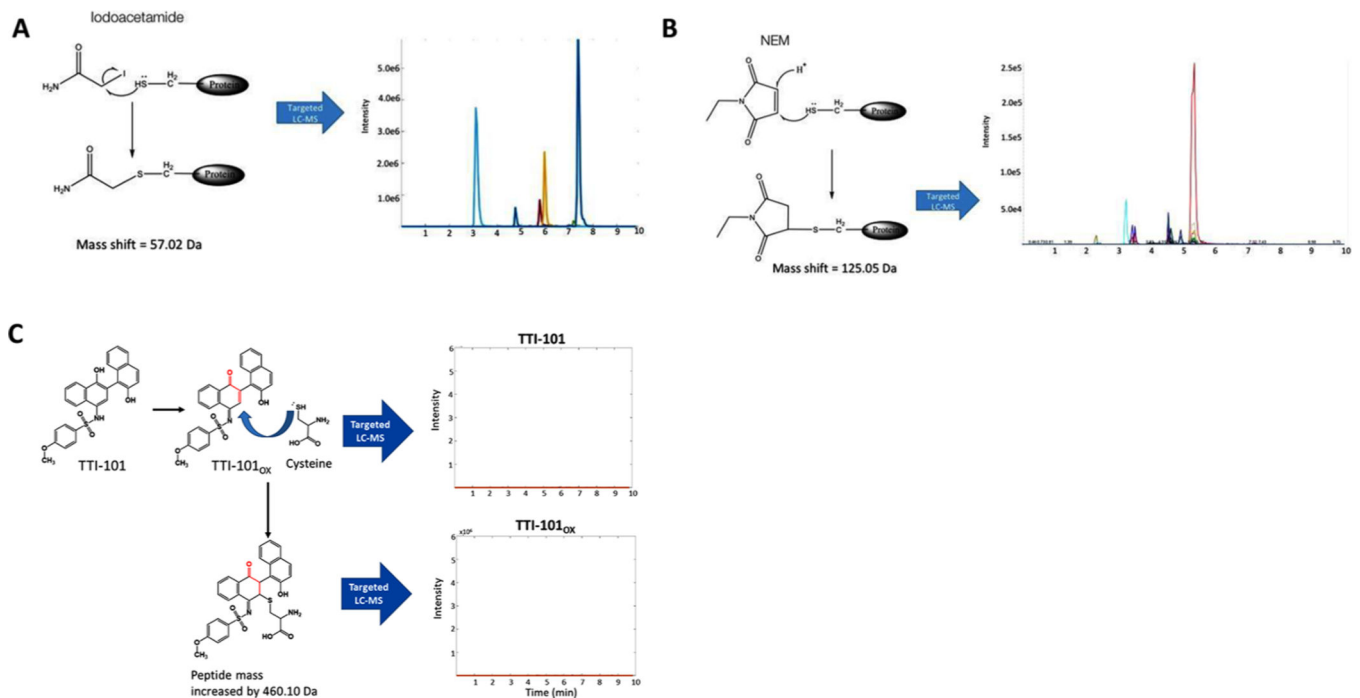


Fig. 3. Stability of compounds incubated with GSH. The AUC of each compound measured at the times indicated by UV-HPLC and expressed as percent of the starting AUC of the peaks. Data are representative of four independently performed experiments.

**Fig. 4.**

Results of alkylation studies of STAT3 by iodoacetamide, NEM and TTI-101. Schematic depicting chemistry of possible alkylation of STAT3 by iodoacetamide the results of LC-MS chromatograms of STAT3 peptides demonstrating alkylated peptides, as predicted from the chemistry. Schematic depicting chemistry of possible alkylation of STAT3 by NEM the results of LC-MS chromatograms of STAT3 peptides demonstrating alkylated peptides, as predicted from the chemistry. Schematic depicting the chemistry of possible alkylation of STAT3 by TTI-101. The LC-MS chromatograms of STAT3 peptides, that, shows no MRM signal for predicted peptide adducts, indicating that no peptides were alkylated.

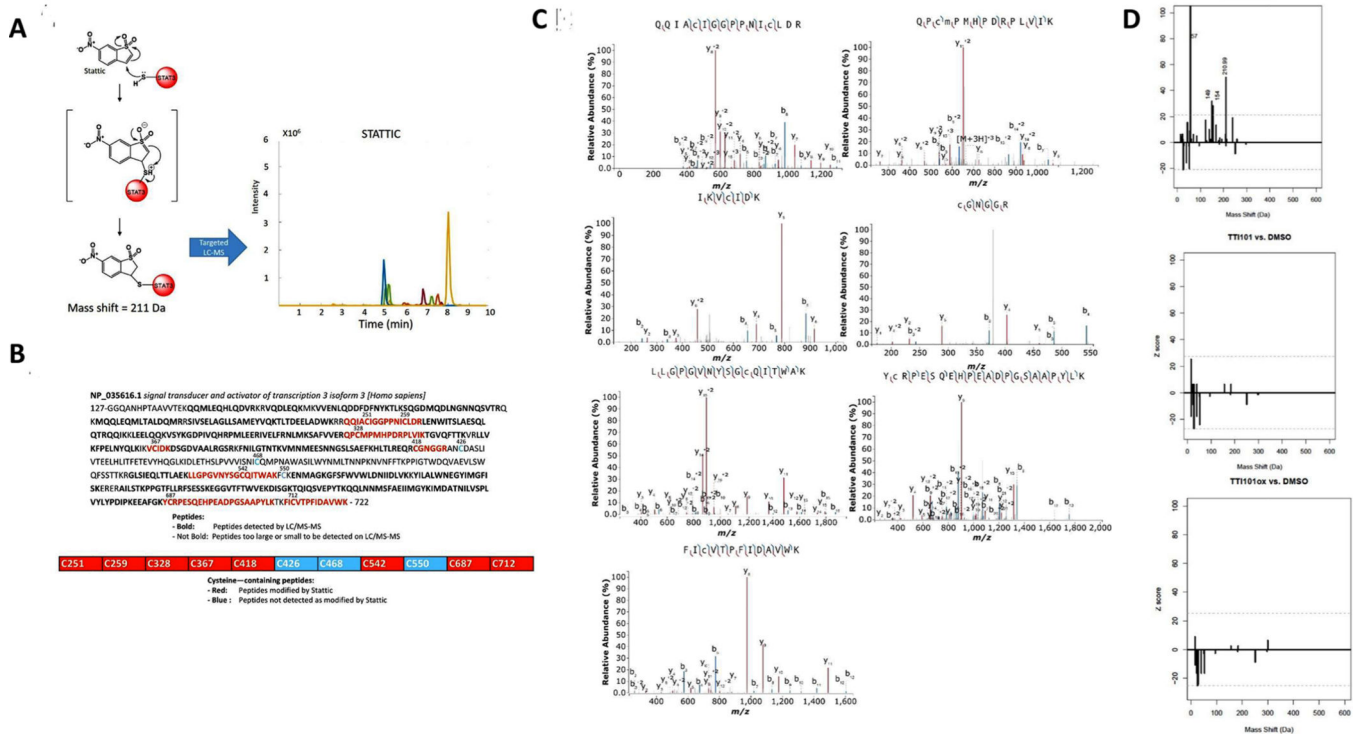
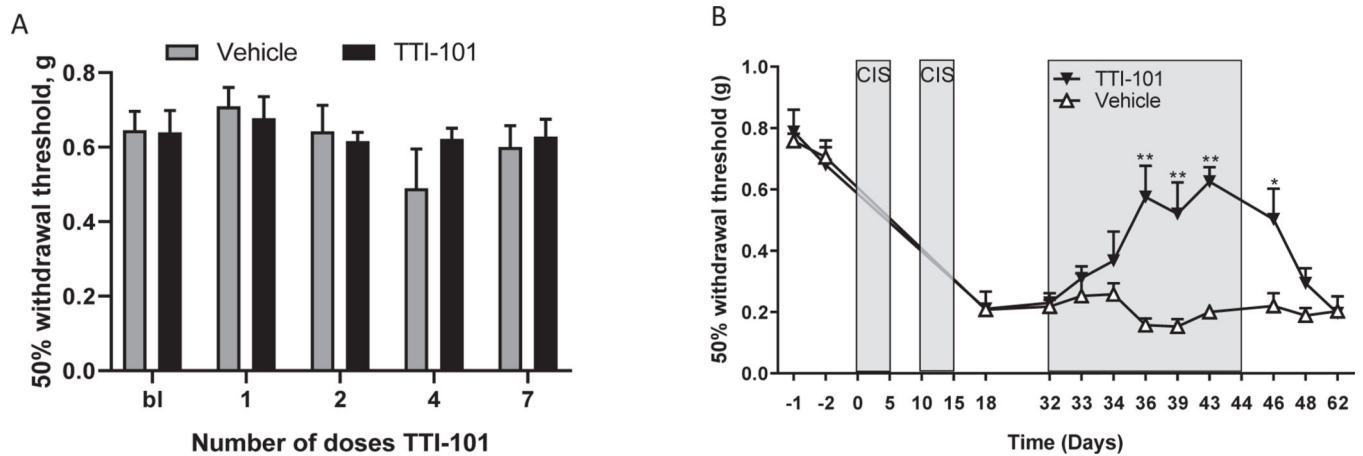


Fig. 5. Alkylation of STAT3 by Static. Schematic depicting chemistry of possible alkylation of STAT3 by Static and results of LC-MS chromatograms of STAT3 peptides of alkylated peptides, as predicted from reaction chemistry. Results of LC-MS/MS demonstrating covalent modification of STAT3 by Static. Chromatograms show fragment ion analysis revealing alkylation of each cysteine-containing peptide, as indicated. Mass Spectra were annotated using IPISA [47]. Representative data of four independent experiments. Amino acid sequence of STAT3βtr indicating cysteine residues modified. Red residues indicates cysteine-containing tryptic fragments identified by LC-MS/MS, with some peptides containing more than one modified cysteine. Bolded residues are within tryptic fragments that can be identified by LC-MS/MS. Residues that are not bolded are within tryptic fragments that are either too large or too small to be detected. Z-score histograms comparing mass shifts of STAT3 peptides incubated with Static, TTI-101, or TTI-101ox vs. STAT3 incubated with DMSO. The dotted line indicates the cutoff for a significant Z-score. The peptide mass peak shifted by 211 Da represents the predicted addition of Static as a chemical adduct; no significant mass shifts were observed with TTI-101 or with TTI-101ox indicating that neither forms chemical adducts with STAT3.

**Fig. 6.**

TTI-101 does not cause mechanical allodynia; rather, it reverses mechanical allodynia caused by cisplatin. A. Male C57/B16 mice (n = 8 per group) received TTI-101 (50 mg/kg i.p. every other day) and mechanical allodynia was assessed using von Frey hairs and the up-and-down method. B. Male C57/B16 mice (n = 4 per group) were treated with cisplatin (two rounds of 5 daily doses of 2.3 mg/kg i.p. followed by 5 days of rest). Dosing with TTI-101 (50 mg/kg i.p. every other day) started 17 days after the last dose of cisplatin. Data were analyzed by two-way ANOVA repeated measures. Time: $P < 0.001$; Group: $P < 0.001$; Interaction $P < 0.001$. ** $P < 0.01$ Tukey multiple comparison test.

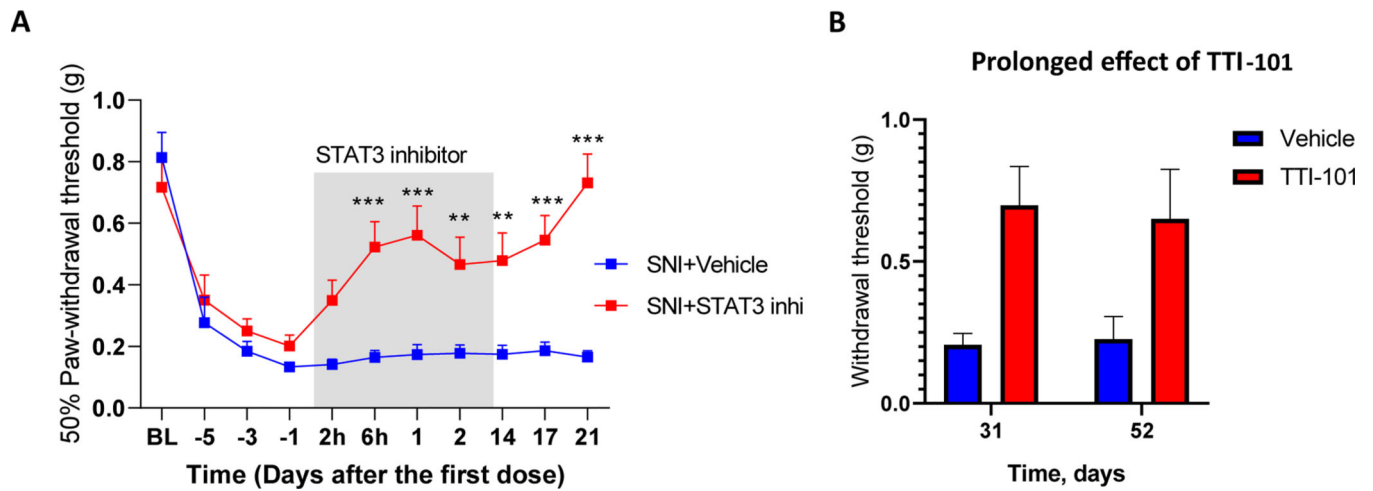


Fig. 7.

STAT3 inhibitor reverses SNI-induced allodynia. Male and female mice underwent SNI surgery and were treated with TTI-101 (Males: $n = 5$; females: $n = 6$) or vehicle (Males: $n = 4$; Females: $n = 6$) by oral gavage for 6 doses every other day from day 10 after SNI. Mechanical allodynia in male and female mice. Data are shown as mean \pm SEM and were analyzed using two-way ANOVA followed by Sidak's post-hoc test. * $P < 0.05$. No signs of mechanical allodynia at 31 and 52 days after start of TTI-101 treatment (19 and 40 days after the last dose). Data are from 4 vehicle-treated and 5 TTI-101-treated male mice per group). Two-way ANOVA followed by Sidak's post-hoc test: $P < 0.05$.

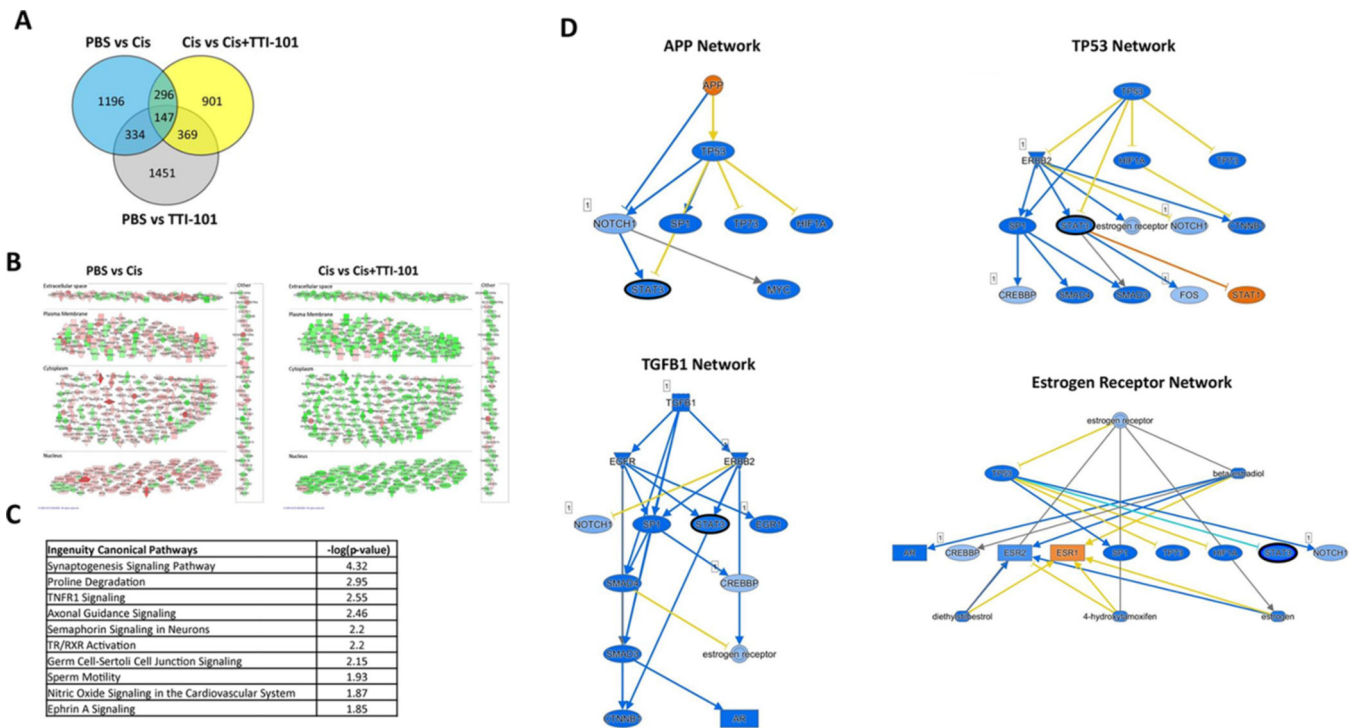


Fig. 8. Effect of TTI-101 on the DRG transcriptome of cisplatin-treated mice. Genes differentially expressed among groups is shown in a Venn diagram. Expression of 1,973 genes was changed in response to cisplatin when compared to the PBS mice (PBS vs. Cis; n = 3 male mice per group). Expression of 1,713 genes was changed in response to TTI-101 administration vs. mice treated with cisplatin alone (Cis vs. Cis + TTI-101). A cutoff of $(-0.2 < \log_2 \text{Fold Change} < 0.2)$ and $p = 0.1$ was used for the analysis. Expression of 2,154 genes was changes in response to TTI-101 administration compared to PBS mice (PBS vs TTI-101). Subcellular clustering of 443 overlapping genes showing directionality of expression. Up-regulated and down-regulated genes are highlighted in red and green, respectively. Gray indicates effect cannot be predicted. Top IPA canonical pathways along with $-\log(p\text{-value})$ assigned to 443 common genes between PBS vs. Cis and Cis vs. Cis + TTI-101 mice. Mechanistic networks of four upstream regulators involving STAT3 as an intermediate regulator. Note that STAT3 (black outline) is an intermediate regulator in all networks and it is predicted to be inhibited. Color orange and blue indicate activation or inhibition respectively. Yellow arrow represents inconsistent relationship when the expected direction is different from direction observed.

A

Upstream Regulators	Z-score	
	PBS vs Cis	Cis vs Cis+TTI-101
Vegf	5.042	-4.641
ERG	4.529	-4.548
SP1	4.409	-3.982
TGFB1	2.206	-5.111
Tgf beta	2.518	-4.701
GATA1	2.928	-4.163
IFNG	2.962	3.609
HGF	3.701	-2.845
PDGF BB	2.647	-3.864
VEGFA	2.511	-3.964

B

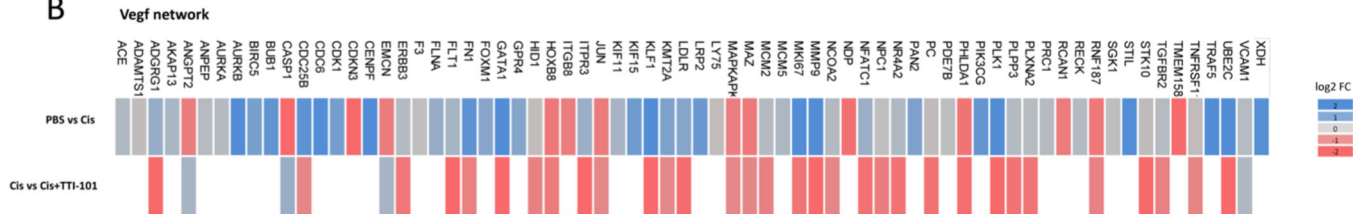


Fig. 9.

Results of IPA comparison analyses. A. Top upstream regulators driving TTI-101-dependent changes in DRG identified using the IPA comparison analysis tool. IPA core analysis was performed between PBS vs. Cisplatin and Cisplatin vs. Cisplatin + TTI-101, followed by comparison of the two core analyses. B. Heat map showing details of target genes in VEGF network. Fold change data for target genes upregulated (blue) or downregulated (red) is shown.

Table 1

Details on the overlapping genes that were altered in both groups, PBS vs Cis, and Cis vs Cis + TTI-101.

Symbol	Entrez Gene Name	Location	PBS vs Cis		Cis vs Cis + TTI-101	
			log ₂ Fold	Expr p-value	log ₂ Fold	Expr p-value
1	6530402F18Rik	RIKEN cDNA 6530402F18 gene	-0.27	0.07	-0.44	0.02
2	ABCA2	ATP binding cassette subfamily A member 2	0.23	0.01	-0.42	0.04
3	ABCA3	ATP binding cassette subfamily A member 3	0.28	0.00	-0.32	0.06
4	ABCA7	ATP binding cassette subfamily A member 7	0.24	0.01	-0.36	0.03
5	ABCG4	ATP binding cassette subfamily G member 4	0.24	0.00	-0.32	0.04
6	ABHD17A	abhydrolase domain containing 17A	-0.23	0.00	-0.35	0.00
7	ABHD8	abhydrolase domain containing 8	-0.27	0.00	-0.21	0.06
8	ACACB	acetyl-CoA carboxylase beta	0.30	0.02	-0.30	0.04
9	ADAMTSL2	ADAMTS like 2	0.37	0.02	-0.31	0.08
10	ADAP1	ArfGAP with dual PH domains 1	-0.22	0.00	-0.23	0.05
11	ADCK2	aarF domain containing kinase 2	0.20	0.05	-0.30	0.02
12	AEBP1	AE binding protein 1	0.60	0.00	-0.23	0.08
13	AKNA	AT-hook transcription factor	0.54	0.00	-0.41	0.03
14	ALAD	aminolevulinate dehydratase	0.30	0.01	-0.43	0.01
15	ALDH2	aldehyde dehydrogenase 2 family member	0.23	0.00	-0.34	0.02
16	ALDH4A1	aldehyde dehydrogenase 4 family member A1	0.35	0.00	-0.29	0.05
17	ALOX5	arachidonate 5-lipoxygenase	0.76	0.00	-0.38	0.07
18	AMBRA1	autophagy and beclin 1 regulator 1	0.22	0.01	-0.32	0.02
19	AMOTL2	angiominin like 2	0.24	0.00	-0.31	0.01
20	AMPD2	adenosine monophosphate deaminase 2	0.24	0.00	-0.25	0.07
21	AMPD3	adenosine monophosphate deaminase 3	0.26	0.00	-0.21	0.08
22	ANKRD13B	ankyrin repeat domain 13B	-0.26	0.01	-0.28	0.05
23	ANO1	anoctamin 1	0.36	0.01	-0.33	0.04
24	AP5Z1	adaptor related protein complex 5 subunit zeta 1	0.24	0.01	-0.27	0.04
25	ARAP3	ArfGAP with RhoGAP domain, ankyrin repeat and PH domain	0.36	0.00	-0.24	0.07
26	ARHGEF10L	Rho guanine nucleotide exchange factor 10 like	-0.34	0.00	-0.28	0.05

Symbol	Entrez Gene Name	Location	PBS vs Cis		Cis vs Cis + TTI-101	
			log ₂ Fold	Expr p-value	log ₂ Fold	Expr p-value
27	ARHGEF2	Rho/Rac guanine nucleotide exchange factor 2	0.28	0.00	-0.22	0.05
28	ARID3A	AT-rich interaction domain 3A	0.29	0.05	-0.29	0.05
29	ARMC7	armadillo repeat containing 7	0.22	0.07	-0.35	0.02
30	ARMH3	armadillo like helical domain containing 3	0.25	0.00	-0.28	0.09
31	ARRDC1	arrestin domain containing 1	0.22	0.01	-0.20	0.08
32	ATP1B2	ATPase Na ⁺ /K ⁺ + transporting subunit beta 2	0.25	0.00	-0.42	0.01
33	ATP2A3	ATPase sarcoplasmic/endoplasmic reticulum Ca ²⁺ + transporting 3	0.53	0.00	-0.49	0.00
34	ATP2B2	ATPase plasma membrane Ca ²⁺ + transporting 2	0.39	0.00	-0.45	0.02
35	ATP6V1G2	ATPase H ⁺ + transporting V1 subunit G2	0.23	0.00	-0.31	0.01
36	B230206H07Rik	RIKEN cDNA B230206H07 gene	0.59	0.00	-0.38	0.07
37	BAG3	BCL2 associated athanogene 3	-0.27	0.00	-0.38	0.01
38	BCAR1	BCAR1 scaffold protein, Cas family member	-0.23	0.03	-0.31	0.05
39	BCOR	BCL6 corepressor	0.28	0.00	-0.21	0.07
40	BRD3	bromodomain containing 3	0.34	0.00	-0.26	0.06
41	BRPF3	bromodomain and PHD finger containing 3	0.26	0.00	-0.22	0.05
42	C11orf24	chromosome 11 open reading frame 24	0.32	0.00	-0.31	0.08
43	C11orf98	chromosome 11 open reading frame 98	-0.24	0.03	0.25	0.04
44	C15orf39	chromosome 15 open reading frame 39	0.37	0.05	-0.50	0.03
45	C1QC	complement C1q C chain	-0.38	0.01	0.52	0.01
46	C3AR1	complement C3a receptor 1	-0.44	0.06	0.63	0.02
47	CACHD1	cache domain containing 1	0.22	0.02	-0.29	0.08
48	CACNG5	calcium voltage-gated channel auxiliary subunit gamma 5	0.41	0.00	-0.47	0.02
49	CAD	carbamoyl-phosphate synthetase 2, aspartate transcarbamylase, and dihydroorotase	0.22	0.03	-0.49	0.01
50	CAMK2B	calcium/calmodulin dependent protein kinase II beta	0.23	0.00	-0.28	0.03
51	CARMIL2	capping protein regulator and myosin 1 linker 2	-0.29	0.00	-0.32	0.02
52	CASPI	caspase 1	-0.36	0.06	0.33	0.06
53	CASR	calcium sensing receptor	-0.36	0.09	0.33	0.07
54	CBLL1	Cbl proto-oncogene like 1	0.24	0.02	-0.30	0.07
55	CCDC88B	coiled-coil domain containing 88B	0.40	0.09	-0.44	0.08

Symbol	Entrez Gene Name	Location	PBS vs Cis		Cis vs Cis + TTI-101	
			log ₂ Fold	Expr p-value	log ₂ Fold	Expr p-value
56	CCDC88C	coiled-coil domain containing 88C	0.88	0.00	-0.44	0.04
57	CCDC92B	coiled-coil domain containing 92B	-0.28	0.00	-0.31	0.03
58	CCN2	cellular communication network factor 2	0.36	0.03	-0.34	0.08
59	CDC42EP3	CDC42 effector protein 3	0.25	0.04	-0.30	0.02
60	CEP250	centrosomal protein 250	0.22	0.00	-0.21	0.07
61	CHD4	chromodomain helicase DNA binding protein 4	0.23	0.00	-0.24	0.08
62	CHD5	chromodomain helicase DNA binding protein 5	0.21	0.00	-0.35	0.01
63	CHERP	calcium homeostasis endoplasmic reticulum protein	0.24	0.01	-0.43	0.00
64	CHIC2	cysteine rich hydrophobic domain 2	-0.21	0.07	0.23	0.08
65	CHPF	chondroitin polymerizing factor	-0.28	0.00	-0.24	0.05
66	CHST2	carbohydrate sulfotransferase 2	-0.25	0.00	-0.31	0.01
67	CIART	circadian associated repressor of transcription	0.53	0.02	0.37	0.04
68	CISD3	CDGSH iron sulfur domain 3	-0.23	0.00	0.21	0.04
69	CITED2	Chp/p300 interacting transactivator with Glu/Asp rich carboxy-terminal domain 2	0.24	0.03	-0.27	0.05
70	CLIP2	CAP-Gly domain containing linker protein 2	-0.21	0.01	-0.33	0.03
71	CLSTN2	calsynenin 2	0.21	0.00	-0.26	0.08
72	CLSTN3	calsynenin 3	0.22	0.01	-0.29	0.07
73	CLUH	clustered mitochondria homolog	0.40	0.00	-0.41	0.03
74	CNTN2	contactin 2	0.24	0.00	-0.41	0.02
75	CNTROB	centrobin, centriole duplication and spindle assembly protein	0.28	0.01	-0.27	0.05
76	COBLL1	cordo-bleu WH2 repeat protein like 1	0.25	0.03	-0.27	0.02
77	COL6A3	collagen type VI alpha 3 chain	0.43	0.00	-0.25	0.08
78	COMP	cartilage oligomeric matrix protein	0.39	0.00	-0.31	0.06
79	CORO6	coronin 6	0.25	0.02	-0.24	0.07
80	CORO7/CORO7-PAMI6	coronin 7	0.32	0.00	-0.29	0.07
81	CPBI	carboxypeptidase B1	-0.26	0.04	0.26	0.06
82	CPSF1	cleavage and polyadenylation specific factor 1	0.54	0.00	-0.30	0.07
83	CRIP1	cysteine rich protein 1	-0.29	0.00	0.29	0.04
84	CRMP1	collapsin response mediator protein 1	0.27	0.00	-0.27	0.07

Symbol	Entrez Gene Name	Location	PBS vs Cis		Cis vs Cis + TTI-101	
			log ₂ Fold	Expr p-value	log ₂ Fold	Expr p-value
85 CRTC2	CREB regulated transcription coactivator 2	Nucleus	0.21	0.00	-0.27	0.01
86 CSDC2	cold shock domain containing C2	Cytoplasm	0.20	0.03	-0.46	0.01
87 CSF3R	colony stimulating factor 3 receptor	Plasma Membrane	0.63	0.00	-0.46	0.07
88 CSMD2	CUB and Sushi multiple domains 2	Other	0.25	0.03	-0.33	0.01
89 CSNK1G2	casein kinase 1 gamma 2	Cytoplasm	-0.23	0.00	-0.24	0.04
90 CSRNPI	cysteine and serine rich nuclear protein 1	Nucleus	0.32	0.07	-0.44	0.02
91 CTSE	cathepsin E	Cytoplasm	1.04	0.02	-0.65	0.00
92 Cux1	cut-like homeobox 1	Nucleus	0.24	0.00	-0.28	0.03
93 CX3CL1	C-X3-C motif chemokine ligand 1	Extracellular Space	0.33	0.01	-0.33	0.06
94 DAG1	dystroglycan 1	Plasma Membrane	0.21	0.00	-0.48	0.01
95 DAP	death associated protein	Cytoplasm	0.21	0.02	-0.23	0.03
96 DDX19A	DEAD-box helicase 19A	Nucleus	0.23	0.02	-0.24	0.06
97 DGCR2	DiGeorge syndrome critical region gene 2	Plasma Membrane	0.20	0.00	-0.27	0.08
98 DGKD	diacylglycerol kinase delta	Cytoplasm	0.23	0.01	-0.21	0.07
99 DHX34	DEXH-box helicase 34	Other	0.24	0.02	-0.33	0.06
10 DIO2	iodothyronine deiodinase 2	Cytoplasm	-0.47	0.04	-0.59	0.01
10 DISPI	dispatched RND transporter family member 1	Plasma Membrane	0.28	0.00	-0.22	0.06
10 DLC1	DLC1 Rho GTPase activating protein	Cytoplasm	0.24	0.00	-0.30	0.07
10 DLGAP3	DLG associated protein 3	Cytoplasm	-0.28	0.01	-0.36	0.05
10 DNAJC15	DnaJ heat shock protein family (Hsp40) member C15	Cytoplasm	-0.22	0.02	0.21	0.09
10 DNMI1	dynamitin 1	Cytoplasm	-0.22	0.03	-0.27	0.09
10 DNMT1	DNA methyltransferase 1	Nucleus	0.38	0.00	-0.24	0.05
10 DOCK1	dedicator of cytokinesis 1	Cytoplasm	0.29	0.00	-0.36	0.02
10 DOCK6	dedicator of cytokinesis 6	Cytoplasm	0.41	0.00	-0.22	0.10

Symbol	Entrez Gene Name	Location	PBS vs Cis		Cis vs Cis + TTF-101	
			log ₂ Fold	Expr p-value	log ₂ Fold	Expr p-value
10 9	DOCK8 dedicator of cytokinesis 8	Cytoplasm	0.45	0.00	-0.30	0.01
11 0	DOK3 docking protein 3	Cytoplasm	0.48	0.02	-0.43	0.07
11 1	DOP1B DOP1 leucine zipper like protein B	Cytoplasm	0.28	0.01	-0.41	0.03
11 2	DPYSL4 dihydropyrimidinase like 4	Cytoplasm	0.34	0.00	-0.25	0.02
11 3	DUS3L dihydrouridine synthase 3 like	Other	0.23	0.00	-0.20	0.05
11 4	DUSP15 dual specificity phosphatase 15	Cytoplasm	0.28	0.01	-0.31	0.05
11 5	E2F2 E2F transcription factor 2	Nucleus	0.52	0.00	-0.33	0.09
11 6	EDC4 enhancer of mRNA decapping 4	Cytoplasm	0.43	0.00	-0.25	0.08
11 7	EFHC1 EF-hand domain containing 1	Cytoplasm	-0.29	0.04	0.34	0.03
11 8	EGR2 early growth response 2	Nucleus	0.28	0.04	-0.52	0.02
11 9	ELANE elastase, neutrophil expressed	Extracellular Space	0.86	0.00	-0.72	0.03
12 0	ELMO1 engulfment and cell motility 1	Cytoplasm	0.26	0.00	-0.22	0.08
12 1	EMC1 ER membrane protein complex subunit 1	Plasma Membrane	0.27	0.00	-0.22	0.10
12 2	EMCN endomucin	Extracellular Space	-0.22	0.02	0.29	0.03
12 3	EPHA2 EPH receptor A2	Plasma Membrane	0.30	0.09	-0.43	0.03
12 4	ERBB2 erb-b2 receptor tyrosine kinase 2	Plasma Membrane	0.26	0.01	-0.35	0.01
12 5	ERBB3 erb-b2 receptor tyrosine kinase 3	Plasma Membrane	0.26	0.00	-0.27	0.01
12 6	ERMAP erythroblast membrane associated protein (Scianna blood group)	Cytoplasm	1.31	0.00	-0.54	0.06

Symbol	Entrez Gene Name	Location	PBS vs Cis		Cis vs Cis + TTI-101	
			log ₂ Fold	Expr p-value	log ₂ Fold	Expr p-value
12 7	ESS2 ess-2 splicing factor homolog	Nucleus	0.28	0.00	-0.22	0.09
12 8	EXOSC9 exosome component 9	Nucleus	-0.20	0.03	0.20	0.09
12 9	F2RL2 coagulation factor II thrombin receptor like 2	Plasma Membrane	-0.23	0.00	0.22	0.04
13 0	F5 coagulation factor V	Extracellular Space	0.76	0.00	-0.45	0.04
13 1	F630028010Rik RIKEN cDNA F630028010 gene	Other	0.82	0.00	-0.47	0.07
13 2	FABP7 fatty acid binding protein 7	Cytoplasm	-0.55	0.00	-0.28	0.03
13 3	FAM20A FAM20A golgi associated secretory pathway pseudokinase	Extracellular Space	0.35	0.00	-0.31	0.04
13 4	FAM222B family with sequence similarity 222 member B	Nucleus	0.41	0.00	-0.36	0.05
13 5	FAM234A family with sequence similarity 234 member A	Plasma Membrane	0.37	0.00	-0.31	0.02
13 6	FAM43B family with sequence similarity 43 member B	Other	-0.25	0.02	-0.35	0.05
13 7	FARSB phenylalanyl-tRNA synthetase subunit beta	Cytoplasm	-0.23	0.00	0.22	0.07
13 8	FAT1 FAT atypical cadherin 1	Plasma Membrane	0.45	0.00	-0.40	0.04
13 9	FBLN1 fibulin 1	Extracellular Space	0.40	0.00	-0.34	0.02
14 0	FBLN7 fibulin 7	Extracellular Space	0.35	0.01	-0.31	0.08
14 1	FBXO42 F-box protein 42	Other	0.21	0.00	-0.28	0.07
14 2	FERMT3 fermitin family member 3	Cytoplasm	0.67	0.00	-0.48	0.06
14 3	FGGY FGGY carbohydrate kinase domain containing	Other	-0.22	0.04	0.24	0.07
14 4	FICD FIC domain containing	Nucleus	0.24	0.00	-0.39	0.02

Symbol	Entrez Gene Name	Location	PBS vs Cis		Cis vs Cis + TTI-101	
			log ₂ Fold	Expr p-value	log ₂ Fold	Expr p-value
14 5	FLOT1 flotillin 1	Plasma Membrane	0.25	0.00	-0.25	0.07
14 6	FLT1 fms related tyrosine kinase 1	Plasma Membrane	0.29	0.00	-0.50	0.00
14 7	FMN2 formin 2	Cytoplasm	-0.24	0.00	-0.26	0.04
14 8	FMNL3 formin like 3	Cytoplasm	0.26	0.05	-0.25	0.09
14 9	Folh1 folate hydrolase 1	Plasma Membrane	-0.28	0.00	0.28	0.01
15 0	FRMPD1 FERM and PDZ domain containing 1	Cytoplasm	0.27	0.00	-0.37	0.04
15 1	FRYL FRY like transcription coactivator	Other	0.43	0.00	-0.24	0.09
15 2	FSCN1 fascin actin-bundling protein 1	Cytoplasm	-0.25	0.02	-0.41	0.00
15 3	GAA glucosidase alpha. acid	Cytoplasm	0.35	0.00	-0.40	0.03
15 4	GAS2L1 growth arrest specific 2 like 1	Cytoplasm	-0.32	0.00	-0.27	0.06
15 5	GATB glutamyl-tRNA amidotransferase subunit B	Cytoplasm	-0.22	0.02	0.22	0.09
15 6	GBF1 golgi brefeldin A resistant guanine nucleotide exchange factor 1	Cytoplasm	0.33	0.00	-0.31	0.10
15 7	GCN1 GCN1 activator of EIF2AK4	Cytoplasm	0.25	0.01	-0.34	0.06
15 8	GDF11 growth differentiation factor 11	Extracellular Space	-0.25	0.00	-0.21	0.05
15 9	GDPD5 glycerophosphodiester phosphodiesterase domain containing 5	Plasma Membrane	-0.25	0.00	-0.22	0.03
16 0	GLRX glutaredoxin	Cytoplasm	-0.20	0.01	0.22	0.06
16 1	Gm12696 predicted gene 12,696	Other	-0.39	0.00	0.27	0.08
16 2	Gm16907 predicted gene, 16,907	Other	0.59	0.01	0.45	0.02

Symbol	Entrez Gene Name	Location	PBS vs Cis		Cis vs Cis + TTI-101	
			log ₂ Fold	Expr p-value	log ₂ Fold	Expr p-value
16 3	GN77 G protein subunit gamma 7	Plasma Membrane	0.23	0.01	-0.38	0.01
16 4	GPC1 glypican 1	Plasma Membrane	-0.20	0.00	-0.23	0.05
16 5	GPD1 glycerol-3-phosphate dehydrogenase 1	Cytoplasm	-0.20	0.03	-0.25	0.02
16 6	GPR153 G protein-coupled receptor 153	Plasma Membrane	-0.25	0.01	-0.26	0.06
16 7	GRINA glutamate ionotropic receptor NMDA type subunit associated protein 1	Other	0.37	0.00	-0.30	0.07
16 8	GTF3A general transcription factor IIIA	Nucleus	0.29	0.04	-0.29	0.07
16 9	GUCY1A1 guanylate cyclase 1 soluble subunit alpha 1	Cytoplasm	0.33	0.01	-0.27	0.05
17 0	GYPC glycophorin C (Gerbich blood group)	Plasma Membrane	0.37	0.00	-0.39	0.01
17 1	HCFC1 host cell factor C1	Nucleus	0.32	0.00	-0.39	0.04
17 2	HCN2 hyperpolarization activated cyclic nucleotide gated potassium and sodium channel 2	Plasma Membrane	-0.35	0.06	-0.33	0.09
17 3	HCN4 hyperpolarization activated cyclic nucleotide gated potassium channel 4	Plasma Membrane	-0.20	0.06	-0.36	0.02
17 4	HDDC2 HD domain containing 2	Cytoplasm	-0.27	0.00	0.22	0.08
17 5	HELZ helicase with zinc finger	Nucleus	0.24	0.01	-0.21	0.09
17 6	HEMGN hemogen	Nucleus	1.31	0.00	-0.69	0.03
17 7	HGF hepatocyte growth factor	Extracellular Space	-0.32	0.00	0.28	0.04
17 8	HHATL hedgehog acyltransferase like	Cytoplasm	0.20	0.04	-0.24	0.09
17 9	HIVEP1 HIVEP zinc finger 1	Nucleus	0.21	0.01	-0.34	0.05
18 0	HOXA7 homeobox A7	Nucleus	0.25	0.01	-0.35	0.02

Symbol	Entrez Gene Name	Location	PBS vs Cis		Cis vs Cis + TTI-101	
			log ₂ Fold	Expr p-value	log ₂ Fold	Expr p-value
18 1	HOXC10	Nucleus	0.29	0.01	-0.28	0.04
18 2	HPS4	Cytoplasm	0.30	0.00	-0.28	0.04
18 3	HSP90AA1	Cytoplasm	-0.26	0.00	0.21	0.07
18 4	Ifi27	Cytoplasm	-0.23	0.00	0.22	0.03
18 5	Ifi2712a/Ifi2712b	Cytoplasm	-0.38	0.02	0.70	0.09
18 6	IFRD2	Nucleus	0.64	0.00	-0.53	0.01
18 7	IGLON5	Other	-0.23	0.01	-0.32	0.02
18 8	INCENP	Nucleus	0.61	0.00	-0.38	0.03
18 9	INPP5E	Cytoplasm	0.21	0.01	-0.20	0.08
19 0	INSRR	Plasma Membrane	0.62	0.01	-0.43	0.04
19 1	INSYN1	Plasma Membrane	-0.32	0.00	-0.31	0.05
19 2	IPO4	Nucleus	0.26	0.00	-0.26	0.09
19 3	IRF2BP1	Nucleus	-0.26	0.01	-0.37	0.03
19 4	IRF2BPL	Nucleus	-0.25	0.01	-0.30	0.05
19 5	ITGA2B	Plasma Membrane	0.47	0.01	-0.61	0.01
19 6	ITPR3	Cytoplasm	0.33	0.00	-0.43	0.02
19 7	KCNA1	Plasma Membrane	0.22	0.01	-0.31	0.07
19 8	KIAA1522	Other	-0.21	0.01	-0.30	0.06

Symbol	Entrez Gene Name	Location	PBS vs Cis		Cis vs Cis + TTI-101	
			log ₂ Fold	Expr p-value	log ₂ Fold	Expr p-value
19 9	KIAA1549L KIAA1549 like	Cytoplasm	0.20	0.01	-0.53	0.00
20 0	KMT2D lysine methyltransferase 2D	Nucleus	0.20	0.08	-0.24	0.06
20 1	KNDC1 kinase non-catalytic C-lobe domain containing 1	Plasma Membrane	0.26	0.01	-0.44	0.03
20 2	LAMA5 laminin subunit alpha 5	Extracellular Space	0.37	0.00	-0.32	0.04
20 3	LAMC3 laminin subunit gamma 3	Extracellular Space	0.49	0.00	-0.50	0.06
20 4	LDLR low density lipoprotein receptor	Plasma Membrane	0.39	0.00	-0.33	0.08
20 5	LGALS1 galectin 1	Extracellular Space	-0.31	0.00	0.26	0.06
20 6	LIMK1 LIM domain kinase 1	Cytoplasm	-0.29	0.00	-0.28	0.03
20 7	LITAF lipopolysaccharide induced TNF factor	Nucleus	0.24	0.00	-0.20	0.05
20 8	LOC proline dehydrogenase 1	Cytoplasm	0.23	0.04	0.49	0.01
20 9	LRP1 LDL receptor related protein 1	Plasma Membrane	0.41	0.00	-0.36	0.01
21 0	LRR32 leucine rich repeat containing 32	Plasma Membrane	0.42	0.01	-0.37	0.10
21 1	LRRK1 leucine rich repeat kinase 1	Cytoplasm	0.27	0.01	-0.22	0.05
21 2	LRRN3 leucine rich repeat neuronal 3	Extracellular Space	-0.22	0.02	0.21	0.07
21 3	LSM7 LSM7 homolog, U6 small nuclear RNA and mRNA degradation associated	Nucleus	-0.25	0.02	0.25	0.07
21 4	MADD MAP kinase activating death domain	Cytoplasm	0.20	0.01	-0.23	0.10
21 5	MAP3K14 mitogen-activated protein kinase kinase kinase 14	Cytoplasm	0.26	0.09	-0.25	0.09
21 6	MAP4K2 mitogen-activated protein kinase kinase kinase 2	Cytoplasm	0.31	0.00	-0.27	0.01

Symbol	Entrez Gene Name	Location	PBS vs Cis		Cis vs Cis + TTI-101	
			log ₂ Fold	Expr p-value	log ₂ Fold	Expr p-value
21 7	MAP7 domain containing 1	Cytoplasm	-0.22	0.01	-0.25	0.05
21 8	mitogen-activated protein kinase 7	Cytoplasm	0.23	0.01	-0.32	0.01
21 9	microtubule affinity regulating kinase 4	Cytoplasm	-0.23	0.06	-0.33	0.08
22 0	microtubule associated serine/threonine kinase family member 4	Other	0.31	0.01	-0.42	0.03
22 1	MCC regulator of WNT signaling pathway	Cytoplasm	0.29	0.00	-0.21	0.06
22 2	mediator of DNA damage checkpoint 1	Nucleus	0.31	0.00	-0.30	0.04
22 3	mediator complex subunit 15	Nucleus	0.36	0.00	-0.37	0.05
22 4	mex-3 RNA binding family member D	Nucleus	-0.28	0.01	-0.29	0.07
22 5	major facilitator superfamily domain containing 2B	Plasma Membrane	0.76	0.00	-0.32	0.08
22 6	matrix metalloproteinase 15	Extracellular Space	-0.28	0.00	-0.44	0.01
22 7	matrix metalloproteinase 9	Extracellular Space	0.86	0.00	-0.80	0.00
22 8	myeloperoxidase	Cytoplasm	1.26	0.00	-0.96	0.03
22 9	mannose receptor C type 2	Plasma Membrane	0.23	0.00	-0.23	0.04
23 0	MAS related GPR family member X4	Plasma Membrane	-0.27	0.01	0.26	0.04
23 1	murine retrovirus integration site 1 homolog	Cytoplasm	0.36	0.00	-0.35	0.04
23 2	MTSS I-BAR domain containing 2	Plasma Membrane	-0.31	0.00	-0.38	0.01
23 3	MAX dimerization protein 1	Nucleus	0.40	0.01	-0.35	0.07
23 4	myosin ID	Cytoplasm	0.33	0.00	-0.32	0.07

Symbol	Entrez Gene Name	Location	PBS vs Cis		Cis vs Cis + TTI-101	
			log ₂ Fold	Expr p-value	log ₂ Fold	Expr p-value
23 5	MYO1F myosin IF	Cytoplasm	0.63	0.00	-0.39	0.06
23 6	MYO7A myosin VIIA	Cytoplasm	0.29	0.00	-0.24	0.08
23 7	MYPOP Myb related transcription factor, partner of profilin	Nucleus	-0.25	0.00	-0.29	0.02
23 8	NAA80 N(alpha)-acetyltransferase 80, NatH catalytic subunit	Cytoplasm	0.25	0.00	-0.38	0.01
23 9	Naip1 (includes others) NLR family, apoptosis inhibitory protein 1	Cytoplasm	0.56	0.01	0.30	0.08
24 0	NAT8L N-acetyltransferase 8 like	Cytoplasm	-0.23	0.00	-0.36	0.02
24 1	NCSTN nicastrin	Plasma Membrane	0.30	0.00	-0.25	0.07
24 2	NDUFA3 NADH:ubiquinone oxidoreductase subunit A3	Cytoplasm	-0.21	0.00	0.22	0.06
24 3	NDUFAF4 NADH:ubiquinone oxidoreductase complex assembly factor 4	Cytoplasm	-0.21	0.01	0.20	0.04
24 4	NECTIN1 nectin cell adhesion molecule 1	Plasma Membrane	-0.42	0.00	-0.36	0.07
24 5	NFAM1 NFAT activating protein with ITAM motif 1	Plasma Membrane	0.81	0.00	-0.43	0.09
24 6	NFATC1 nuclear factor of activated T cells 1	Nucleus	0.32	0.01	-0.30	0.05
24 7	NFE2 nuclear factor, erythroid 2	Nucleus	1.09	0.00	-0.61	0.03
24 8	NLGN2 neuroligin 2	Plasma Membrane	-0.25	0.01	-0.32	0.03
24 9	NLGN3 neuroligin 3	Plasma Membrane	0.33	0.00	-0.34	0.00
25 0	NMD3 NMD3 ribosome export adaptor	Nucleus	-0.21	0.01	0.26	0.01
25 1	NOL6 nucleolar protein 6	Nucleus	0.25	0.00	-0.39	0.05
25 2	NOTCH2 notch receptor 2	Plasma Membrane	0.31	0.00	-0.27	0.01

Symbol	Entrez Gene Name	Location	PBS vs Cis		Cis vs Cis + TTF-101	
			log ₂ Fold	Expr p-value	log ₂ Fold	Expr p-value
25 3	Nppb natriuretic peptide type B	Other	-0.40	0.02	0.34	0.05
25 4	NPTXR neuronal pentraxin receptor	Plasma Membrane	-0.22	0.01	-0.29	0.08
25 5	NR1D1 nuclear receptor subfamily 1 group D member 1	Nucleus	0.36	0.01	-0.29	0.02
25 6	NR4A2 nuclear receptor subfamily 4 group A member 2	Nucleus	0.27	0.03	-0.29	0.09
25 7	NRSN2 neurensin 2	Plasma Membrane	0.58	0.00	-0.38	0.07
25 8	NRXN2 neurexin 2	Plasma Membrane	-0.26	0.01	-0.32	0.06
25 9	NUDCD1 NudC domain containing 1	Nucleus	-0.20	0.02	0.20	0.07
26 0	NUMA1 nuclear mitotic apparatus protein 1	Nucleus	0.34	0.00	-0.26	0.08
26 1	NUP188 nucleoporin 188	Nucleus	0.29	0.00	-0.21	0.08
26 2	OGDH oxoglutarate dehydrogenase	Cytoplasm	0.36	0.00	-0.34	0.05
26 3	OGDHL oxoglutarate dehydrogenase like	Other	0.25	0.01	-0.27	0.08
26 4	OLFM2 olfactomedin 2	Cytoplasm	0.31	0.00	-0.25	0.04
26 5	OPRM1 opioid receptor mu 1	Plasma Membrane	-0.28	0.00	0.23	0.01
26 6	OSBPL7 oxysterol binding protein like 7	Cytoplasm	0.27	0.00	-0.26	0.03
26 7	P2RY2 purinergic receptor P2Y2	Plasma Membrane	0.31	0.00	-0.30	0.07
26 8	PALM paralemmin	Plasma Membrane	-0.30	0.00	-0.27	0.05
26 9	PAPLN papilin, proteoglycan like sulfated glycoprotein	Extracellular Space	0.20	0.09	-0.34	0.08
27 0	PC pyruvate carboxylase	Cytoplasm	0.21	0.00	-0.30	0.04

Symbol	Entrez Gene Name	Location	PBS vs Cis		Cis vs Cis + TTI-101	
			log ₂ Fold	Expr p-value	log ₂ Fold	Expr p-value
27 1	PDX1 C-terminal inhibiting factor 1	Nucleus	0.25	0.01	-0.34	0.04
27 2	pecanex 2	Other	0.24	0.01	-0.37	0.04
27 3	proprotein convertase subtilisin/kexin type 1 inhibitor	Extracellular Space	-0.32	0.10	-0.36	0.05
27 4	phosphodiesterase 4A	Cytoplasm	0.32	0.01	-0.39	0.02
27 5	platelet derived growth factor receptor beta	Plasma Membrane	0.54	0.00	-0.27	0.09
27 6	pyruvate dehydrogenase kinase 2	Cytoplasm	0.37	0.00	-0.31	0.10
27 7	PPARGC1 and ESRR induced regulator, muscle 1	Other	0.52	0.01	-0.37	0.08
27 8	phosphoglycolate phosphatase	Cytoplasm	-0.35	0.00	-0.29	0.02
27 9	phosphatase and actin regulator 4	Plasma Membrane	0.24	0.05	-0.26	0.07
28 0	pleckstrin homology like domain family A member 1	Cytoplasm	-0.28	0.05	-0.32	0.05
28 1	PHD and ring finger domains 1	Nucleus	0.28	0.00	-0.32	0.06
28 2	phytanoyl-CoA 2-hydroxylase interacting protein	Cytoplasm	0.34	0.03	-0.45	0.08
28 3	protein inhibitor of activated STAT 3	Nucleus	0.25	0.00	-0.20	0.04
28 4	phosphatidylinositol-4,5-bisphosphate 3-kinase catalytic	Cytoplasm	0.24	0.00	-0.41	0.01
28 5	subunit delta phospholipase A2 receptor 1	Plasma Membrane	-0.21	0.04	0.24	0.09
28 6	PLAG1 like zinc finger 2	Nucleus	0.43	0.00	-0.31	0.06
28 7	pleckstrin homology and RUN domain containing M1	Cytoplasm	0.29	0.00	-0.26	0.06
28 8	phospholipid phosphatase 3	Plasma Membrane	0.26	0.00	-0.29	0.05

Symbol	Entrez Gene Name	Location	PBS vs Cis		Cis vs Cis + TTI-101		
			log ₂ Fold	Expr p-value	log ₂ Fold	Expr p-value	
28 9	PLRG1	pleiotropic regulator 1	Nucleus	-0.21	0.01	0.21	0.07
29 0	PLTP	phospholipid transfer protein	Extracellular Space	0.49	0.00	-0.30	0.04
29 1	PLXNA2	plexin A2	Plasma Membrane	0.25	0.00	-0.28	0.08
29 2	PLXNB1	plexin B1	Plasma Membrane	0.28	0.02	-0.36	0.02
29 3	PLXNB3	plexin B3	Plasma Membrane	0.38	0.00	-0.30	0.05
29 4	PMEPA1	prostate transmembrane protein, androgen induced 1	Plasma Membrane	-0.27	0.00	-0.33	0.01
29 5	POLR2A	RNA polymerase II subunit A	Nucleus	0.21	0.06	-0.44	0.02
29 6	POR	cytochrome p450 oxidoreductase	Cytoplasm	0.41	0.00	-0.33	0.04
29 7	PPEF1	protein phosphatase with EF-hand domain 1	Extracellular Space	-0.22	0.00	0.23	0.02
29 8	PPP1R10	protein phosphatase 1 regulatory subunit 10	Nucleus	0.26	0.00	-0.58	0.01
29 9	PPP1R3E	protein phosphatase 1 regulatory subunit 3E	Cytoplasm	-0.28	0.04	-0.30	0.09
30 0	PPP1R9B	protein phosphatase 1 regulatory subunit 9B	Cytoplasm	-0.34	0.00	-0.26	0.04
30 1	PRELP	proline and arginine rich end leucine rich repeat protein	Extracellular Space	0.35	0.00	-0.25	0.07
30 2	Prrx11	paired related homeobox protein-like 1	Other	0.24	0.00	-0.29	0.06
30 3	PRTN3	proteinase 3	Extracellular Space	0.58	0.01	-0.45	0.09
30 4	PSMA5	proteasome subunit alpha 5	Cytoplasm	-0.22	0.00	0.21	0.05
30 5	PSMB10	proteasome subunit beta 10	Cytoplasm	-0.22	0.08	0.29	0.10
30 6	PSMB3	proteasome subunit beta 3	Cytoplasm	-0.22	0.00	0.22	0.03

Symbol	Entrez Gene Name	Location	PBS vs Cis		Cis vs Cis + TTI-101	
			log ₂ Fold	Expr p-value	log ₂ Fold	Expr p-value
30 7	PSMB7 proteasome subunit beta 7	Cytoplasm	-0.21	0.00	0.20	0.05
30 8	PTPRU protein tyrosine phosphatase receptor type U	Plasma Membrane	0.37	0.00	-0.32	0.04
30 9	PXN paxillin	Cytoplasm	0.25	0.01	-0.25	0.08
31 0	RAB4A RAB4A, member RAS oncogene family	Cytoplasm	0.24	0.00	-0.25	0.04
31 1	RASL10B RAS like family 10 member B	Other	-0.21	0.00	-0.28	0.05
31 2	RAVER1 ribonucleoprotein, PTB binding 1	Nucleus	0.22	0.03	-0.48	0.01
31 3	RBM38 RNA binding motif protein 38	Nucleus	0.85	0.00	-0.57	0.02
31 4	RCC2 regulator of chromosome condensation 2	Nucleus	-0.21	0.00	-0.26	0.07
31 5	RCSD1 RCSD domain containing 1	Other	0.22	0.02	-0.23	0.06
31 6	REEP4 receptor accessory protein 4	Cytoplasm	0.33	0.01	-0.27	0.06
31 7	REEP6 receptor accessory protein 6	Plasma Membrane	0.38	0.04	-0.41	0.07
31 8	RELN reelin	Extracellular Space	0.28	0.00	-0.38	0.03
31 9	Retnlg resistin like gamma	Extracellular Space	0.49	0.07	-0.34	0.08
32 0	RFXANK regulatory factor X associated ankyrin containing protein	Nucleus	0.20	0.09	-0.21	0.08
32 1	RHCE/RHD Rh blood group D antigen	Plasma Membrane	1.07	0.02	-0.54	0.05
32 2	RHOT2 ras homolog family member T2	Cytoplasm	0.20	0.00	-0.21	0.05
32 3	Rn18s-rs5 18 s RNA, related sequence 5	Other	-0.98	0.00	0.79	0.06
32 4	RNF123 ring finger protein 123	Cytoplasm	0.32	0.00	-0.27	0.09

Symbol	Entrez Gene Name	Location	PBS vs Cis		Cis vs Cis + TIT-101	
			log ₂ Fold	Expr p-value	log ₂ Fold	Expr p-value
32 5	RNF208 ring finger protein 208	Other	-0.22	0.02	-0.35	0.02
32 6	RNF216 ring finger protein 216	Cytoplasm	0.33	0.00	-0.36	0.08
32 7	RPAPI RNA polymerase II associated protein 1	Other	0.33	0.00	-0.34	0.03
32 8	RPHE3A rabphilin 3A	Plasma Membrane	0.21	0.01	-0.50	0.01
32 9	Rpl2211 ribosomal protein L22 like 1	Other	-0.27	0.00	0.20	0.06
33 0	RPL26 ribosomal protein L26	Cytoplasm	-0.21	0.00	0.22	0.04
33 1	RPL37A ribosomal protein L37a	Cytoplasm	-0.21	0.00	0.22	0.04
33 2	RPS6KA1 ribosomal protein S6 kinase A1	Cytoplasm	0.32	0.00	-0.42	0.01
33 3	RRM2 ribonucleotide reductase regulatory subunit M2	Nucleus	0.91	0.00	-0.44	0.03
33 4	RTN4R reticulon 4 receptor	Plasma Membrane	-0.22	0.08	-0.26	0.07
33 5	RXRG retinoid X receptor gamma	Nucleus	0.28	0.00	-0.21	0.08
33 6	SAMD14 sterile alpha motif domain containing 14	Other	-0.21	0.01	-0.28	0.03
33 7	SAP130 Sin3A associated protein 130	Nucleus	0.42	0.00	-0.24	0.09
33 8	SCG2 secretogranin II	Extracellular Space	-0.22	0.01	0.20	0.08
33 9	SCN5A sodium voltage-gated channel alpha subunit 5	Plasma Membrane	0.23	0.05	-0.31	0.05
34 0	SCRT1 scratch family transcriptional repressor 1	Nucleus	-0.23	0.04	-0.41	0.02
34 1	SCUBE1 signal peptide, CUB domain and EGF like domain containing 1	Plasma Membrane	0.26	0.01	-0.48	0.02
34 2	SDC3 syndecan 3	Plasma Membrane	-0.22	0.00	-0.25	0.07

Symbol	Entrez Gene Name	Location	PBS vs Cis		Cis vs Cis + TTI-101	
			log ₂ Fold	Expr p-value	log ₂ Fold	Expr p-value
34 3	SEC24 homolog C, COPII coat complex component	Cytoplasm	0.20	0.00	-0.29	0.03
34 4	semaphorin 4B	Plasma Membrane	0.28	0.00	-0.23	0.07
34 5	semaphorin 4G	Plasma Membrane	0.32	0.01	-0.47	0.00
34 6	septin 8	Extracellular Space	0.21	0.00	-0.23	0.05
34 7	serpin family A member 3	Extracellular Space	-0.30	0.00	0.23	0.01
34 8	serine (or cysteine) peptidase inhibitor, clade A, member 3G others	Cytoplasm	-0.49	0.01	0.22	0.03
34 9	serpin family B member 1	Cytoplasm	-0.36	0.00	0.21	0.07
35 0	Serpina1b	Other	-0.23	0.01	0.22	0.08
35 1	seizure related 6 homolog like	Plasma Membrane	0.41	0.00	-0.59	0.01
35 2	secreted frizzled related protein 5	Plasma Membrane	-0.21	0.00	-0.30	0.00
35 3	SH2 domain containing 3C	Cytoplasm	0.23	0.00	-0.24	0.10
35 4	serine hydroxymethyltransferase 2	Cytoplasm	0.23	0.02	-0.27	0.05
35 5	SIX homeobox 5	Nucleus	0.32	0.09	-0.34	0.09
35 6	Skil2 like RNA helicase	Nucleus	0.21	0.00	-0.32	0.03
35 7	solute carrier family 16 member 10	Plasma Membrane	0.51	0.03	-0.45	0.05
35 8	solute carrier family 25 member 37	Cytoplasm	0.64	0.00	-0.24	0.08
35 9	solute carrier family 40 member 1	Plasma Membrane	0.56	0.00	-0.33	0.06
36 0	solute carrier family 4 member 11	Plasma Membrane	0.29	0.00	-0.28	0.04

Symbol	Entrez Gene Name	Location	PBS vs Cis		Cis vs Cis + TTI-101	
			log ₂ Fold	Expr p-value	log ₂ Fold	Expr p-value
36 1	SLC7A8 solute carrier family 7 member 8	Plasma Membrane	0.48	0.00	-0.36	0.07
36 2	SLC9A1 solute carrier family 9 member A1	Plasma Membrane	0.23	0.01	-0.42	0.04
36 3	SLIT1 slit guidance ligand 1	Extracellular Space	0.24	0.01	-0.36	0.06
36 4	SLX4 SLX4 structure-specific endonuclease subunit	Nucleus	0.39	0.00	-0.24	0.06
36 5	SMTN smoothelin	Extracellular Space	0.49	0.00	-0.37	0.03
36 6	SNCB synuclein beta	Cytoplasm	-0.32	0.00	-0.25	0.06
36 7	SNPH synphilin	Plasma Membrane	0.22	0.00	-0.31	0.02
36 8	SOBP sine oculis binding protein homolog	Nucleus	-0.23	0.01	-0.34	0.02
36 9	SOD3 superoxide dismutase 3	Extracellular Space	0.41	0.00	-0.49	0.02
37 0	SOX6 SRY-box transcription factor 6	Nucleus	0.24	0.04	-0.30	0.04
37 1	Spaca6 sperm acrosome associated 6	Other	0.42	0.02	0.33	0.04
37 2	SPECC1 sperm antigen with calponin homology and coiled-coil domains 1	Nucleus	0.22	0.05	-0.26	0.07
37 3	SPIRE2 spire type actin nucleation factor 2	Cytoplasm	-0.31	0.00	-0.27	0.02
37 4	SPSB3 sp/A/ryanodine receptor domain and SOCS box containing 3	Cytoplasm	0.23	0.06	-0.34	0.03
37 5	SPTBN5 spectrin beta, non-erythrocytic 5	Plasma Membrane	0.32	0.01	-0.36	0.05
37 6	SRCAP Snf2 related CREBBP activator protein	Cytoplasm	0.20	0.10	-0.31	0.02
37 7	ST5 suppression of tumorigenicity 5	Cytoplasm	0.26	0.00	-0.25	0.09
37 8	STK10 serine/threonine kinase 10	Cytoplasm	0.21	0.03	-0.36	0.00

Symbol	Entrez Gene Name	Location	PBS vs Cis		Cis vs Cis + TTI-101	
			log ₂ Fold	Expr p-value	log ₂ Fold	Expr p-value
37 9	STUB1 STUB1 homology and U-box containing protein 1	Cytoplasm	0.24	0.00	-0.23	0.05
38 0	SUGP1 SURF and G-patch domain containing 1	Nucleus	0.32	0.00	-0.21	0.06
38 1	SYT2 synaptotagmin 2	Cytoplasm	0.24	0.01	-0.43	0.03
38 2	TAFA5 TAFA chemokine like family member 5	Extracellular Space	-0.25	0.00	-0.24	0.05
38 3	TBC1D17 TBC1 domain family member 17	Cytoplasm	0.24	0.00	-0.29	0.08
38 4	TCOF1 treacle ribosome biogenesis factor 1	Nucleus	0.23	0.07	-0.43	0.05
38 5	TECPR2 tectonin beta-propeller repeat containing 2	Other	0.20	0.01	-0.25	0.08
38 6	TENM2 teneurin transmembrane protein 2	Plasma Membrane	0.42	0.00	-0.28	0.08
38 7	TENM3 teneurin transmembrane protein 3	Plasma Membrane	0.26	0.00	-0.34	0.05
38 8	TENM4 teneurin transmembrane protein 4	Plasma Membrane	0.20	0.06	-0.46	0.02
38 9	TGFB1I1 transforming growth factor beta 1 induced transcript 1	Nucleus	0.35	0.00	-0.36	0.01
39 0	THBS1 thrombospondin 1	Extracellular Space	0.68	0.00	-0.24	0.02
39 1	THEM6 thioesterase superfamily member 6	Other	-0.23	0.00	-0.32	0.02
39 2	TIAM1 T cell lymphoma invasion and metastasis 1	Cytoplasm	0.30	0.00	-0.44	0.01
39 3	TINAGL1 tubulointerstitial nephritis antigen like 1	Extracellular Space	0.28	0.01	-0.35	0.03
39 4	TLN1 talin 1	Plasma Membrane	0.39	0.00	-0.39	0.05
39 5	TMEM151B transmembrane protein 151B	Other	-0.30	0.00	-0.27	0.07
39 6	TMEM160 transmembrane protein 160	Cytoplasm	-0.25	0.02	0.24	0.07

Symbol	Entrez Gene Name	Location	PBS vs Cis		Cis vs Cis + TIT-101		
			log ₂ Fold	Expr p-value	log ₂ Fold	Expr p-value	
39 7	TMEM205	transmembrane protein 205	Cytoplasm	-0.26	0.00	0.23	0.08
39 8	TNFAIP2	TNF alpha induced protein 2	Extracellular Space	0.53	0.00	-0.42	0.06
39 9	TNFRSF1A	TNF receptor superfamily member 1A	Plasma Membrane	0.23	0.01	-0.29	0.08
40 0	TNIP1	TNFAIP3 interacting protein 1	Nucleus	0.21	0.02	-0.38	0.01
40 1	TNXB	tenascin XB	Extracellular Space	0.26	0.01	-0.27	0.02
40 2	TOML2	target of myb1 like 2 membrane trafficking protein	Cytoplasm	0.21	0.00	-0.29	0.05
40 3	TONSL	tonsoku like, DNA repair protein	Cytoplasm	0.43	0.00	-0.38	0.05
40 4	TPRA1	transmembrane protein adipocyte associated 1	Plasma Membrane	0.28	0.00	-0.30	0.00
40 5	TPRN	taperin	Extracellular Space	-0.28	0.02	-0.26	0.08
40 6	TRPA1	transient receptor potential cation channel subfamily A member 1	Plasma Membrane	-0.31	0.00	0.29	0.02
40 7	TRPC6	transient receptor potential cation channel subfamily C member 6	Plasma Membrane	-0.20	0.04	0.29	0.01
40 8	TRPM2	transient receptor potential cation channel subfamily M member 2	Plasma Membrane	0.26	0.00	-0.23	0.05
40 9	TERRAP	transformation/transcription domain associated protein	Nucleus	0.37	0.00	-0.25	0.05
41 0	TSPAN18	tetraspanin 18	Other	0.25	0.00	-0.27	0.08
41 1	TSPAN33	tetraspanin 33	Plasma Membrane	0.46	0.02	-0.35	0.07
41 2	TTBK1	tau tubulin kinase 1	Other	-0.26	0.00	-0.40	0.02
41 3	TTC9B	tetratricopeptide repeat domain 9B	Other	-0.38	0.00	-0.24	0.09
41 4	TTL3	tubulin tyrosine ligase like 3	Extracellular Space	0.61	0.00	-0.36	0.04

Symbol	Entrez Gene Name	Location	PBS vs Cis		Cis vs Cis + TIT-101	
			log ₂ Fold	Expr p-value	log ₂ Fold	Expr p-value
41 5	TTYH3 tweety family member 3	Plasma Membrane	-0.21	0.02	-0.23	0.09
41 6	UBC ubiquitin C	Cytoplasm	0.58	0.00	-0.40	0.05
41 7	UBE3B ubiquitin protein ligase E3B	Extracellular Space	0.31	0.00	-0.38	0.05
41 8	UBL7 ubiquitin like 7	Other	0.22	0.02	-0.25	0.10
41 9	UFSP2 UFM1 specific peptidase 2	Other	-0.22	0.00	0.20	0.06
42 0	ULK3 unc-51 like kinase 3	Cytoplasm	0.27	0.00	-0.22	0.05
42 1	UNC5A unc-5 netrin receptor A	Plasma Membrane	-0.27	0.05	-0.33	0.07
42 2	USP10 ubiquitin specific peptidase 10	Cytoplasm	0.31	0.00	-0.30	0.08
42 3	USP19 ubiquitin specific peptidase 19	Cytoplasm	0.20	0.01	-0.24	0.06
42 4	VGf VGF nerve growth factor inducible	Extracellular Space	-0.73	0.00	-0.35	0.07
42 5	VPS18 VPS18 core subunit of CORVET and HOPS complexes	Cytoplasm	0.22	0.02	-0.35	0.05
42 6	VPS9D1 VPS9 domain containing 1	Other	0.22	0.01	-0.29	0.05
42 7	VWA5A von Willebrand factor A domain containing 5A	Nucleus	-0.28	0.00	0.24	0.02
42 8	WASF1 WASP family member 1	Nucleus	-0.27	0.02	-0.29	0.06
42 9	WBP2 WW domain binding protein 2	Cytoplasm	0.28	0.00	-0.36	0.04
43 0	WDFY3 WD repeat and FYVE domain containing 3	Cytoplasm	0.22	0.01	-0.37	0.03
43 1	YLPMI YLP motif containing 1	Nucleus	0.25	0.00	-0.24	0.02
43 2	ZDHC18 zinc finger DHHC-type containing 18	Cytoplasm	-0.23	0.01	-0.29	0.05

Symbol	Entrez Gene Name	Location	PBS vs Cis		Cis vs Cis + TTF-101	
			log ₂ Fold	Expr p-value	log ₂ Fold	Expr p-value
43 3	ZFP36L1	Nucleus	0.23	0.03	-0.25	0.10
43 4	Zfp651	Other	-0.23	0.00	-0.21	0.03
43 5	ZFYVE26	Cytoplasm	0.44	0.00	-0.28	0.05
43 6	ZNF142	Nucleus	0.30	0.00	-0.23	0.09
43 7	ZNF219	Nucleus	-0.21	0.01	-0.28	0.02
43 8	ZNF423	Nucleus	0.26	0.01	-0.46	0.01
43 9	ZNF442	Nucleus	-0.22	0.05	0.35	0.09
44 0	ZNF592	Nucleus	0.27	0.01	-0.29	0.05
44 1	ZNF646	Nucleus	0.26	0.00	-0.26	0.04
44 2	ZNF703	Nucleus	-0.30	0.00	-0.27	0.07
44 3	ZSWIM1	Nucleus	0.35	0.00	-0.40	0.05

Table 2

Top five upstream regulators and their mechanistic network for differentially expressed.

Upstream Regulator	Activation z-score	Overlap p-value	Mechanistic Network	Other Regulators in mechanistic network
1 HTT	-0.152	1.3E-10		
2 APP	2.394	1.67E-10	431 (8)	TP53, NOTCH1, SP1, TP73, HIF1A, MYC, STAT3
3 TP53	-2.078	1.77E-10	481 (14)	STAT3, ERBB2, TP73, HIF1A, SP1, ESTROGEN RECEPTOR, NOTCH1, CTNNB1, CREBBP, SMAD4, SMAD3, FOS, STAT1
4 TGFB1	-5.111	2.84E-09	436 (13)	EGFP, ERBB2, NOTCH1, SP1, STAT3, EGFR1, SMAD4, CREBBP, SMAD3, ESTROGEN RECEPTOR, CTNNB1, AR
5 estrogen receptor	-0.614	6.22E-09	558 (15)	TP53, BETA-ESTRADIOL, AR, CREBBP, ESR2, ESR1, SP1, TP73, HIF1A, STAT3, NOTCH1, DIETHYLSTILBESTEROL, 4-HYDROXYTAMOXIFEN, ESTROGEN

genes in cisplatin dataset (cisplatin vs. cisplatin + TTI-101). Note, the number in the mechanistic network column denotes the number of target genes influenced by that particular regulator. The number in parenthesis denotes the total number of regulators in that mechanistic network.